9660–9680 *Nucleic Acids Research, 2020, Vol. 48, No. 17* *Published online 5 September 2020*
doi: 10.1093/nar/gkaa686

Genome maintenance functions of a putative *Trypanosoma brucei* translesion DNA polymerase include telomere association and a role in antigenic variation

Andrea Zurita Leal[1,†], Marie Schwebs[2,†], Emma Briggs[1], Nadine Weisert[2], Helena Reis[2], Leandro Lemgruber[1], Katarina Luko[3], Jonathan Wilkes[1], Falk Butter[3], Richard McCulloch[1,*] and Christian J. Janzen[2,*]

[1]The Wellcome Centre for Integrative Parasitology, Institute of Infection, Immunity and Inflammation, University of Glasgow, Glasgow, UK, [2]Department of Cell & Developmental Biology, Biocenter, University of Würzburg, Würzburg, Germany and [3]Quantitative Proteomics, Institute of Molecular Biology (IMB), Mainz, Germany

Received September 25, 2019; Revised August 03, 2020; Editorial Decision August 05, 2020; Accepted September 03, 2020

ABSTRACT

Maintenance of genome integrity is critical to guarantee transfer of an intact genome from parent to offspring during cell division. DNA polymerases (Pols) provide roles in both replication of the genome and the repair of a wide range of lesions. Amongst replicative DNA Pols, translesion DNA Pols play a particular role: replication to bypass DNA damage. All cells express a range of translesion Pols, but little work has examined their function in parasites, including whether the enzymes might contribute to host-parasite interactions. Here, we describe a dual function of one putative translesion Pol in African trypanosomes, which we now name TbPolIE. Previously, we demonstrated that TbPolIE is associated with telomeric sequences and here we show that RNAi-mediated depletion of TbPolIE transcripts results in slowed growth, altered DNA content, changes in cell morphology, and increased sensitivity to DNA damaging agents. We also show that TbPolIE displays pronounced localization at the nuclear periphery, and that its depletion leads to chromosome segregation defects and increased levels of endogenous DNA damage. Finally, we demonstrate that TbPolIE depletion leads to deregulation of telomeric variant surface glycoprotein genes, linking the function of this putative translesion DNA polymerase to host immune evasion by antigenic variation.

INTRODUCTION

Accurate duplication of the genome is a critical component of the cell cycle of all organisms. Two pathways contribute to accurate genome duplication: copying of the genome, and repair of DNA damage. Eukaryotic cells encode a wide range of DNA polymerases (Pols) that are required for DNA synthesis, allowing genome duplication, and for repair of DNA damage (review in (1)). Eukaryotic DNA Pols are divided into four different families (A, B, X and Y) based on sequence and structural homologies. Nuclear DNA Pols that direct the accurate copying of the genome belong to the B family, while mitochondrial genome replication is catalysed by an A family DNA Pol (2). DNA Pols that act in DNA repair span all families, as do so-called translesion DNA Pols, which straddle DNA repair and replication activities because their activity is required whenever replicative DNA Pols encounter lesions in the template strand that must be bypassed to allow genome duplication (3–5). In general, DNA replication is a high fidelity process with an extremely low error rate (6). This is due to a combination of the ability of replicative DNA Pols to efficiently select the correct nucleotide to incorporate into the newly synthesized DNA strand and proofreading activity of the Pols, which permits the excision of occasionally incorrectly inserted nucleotides. Additionally, post-replicative repair mechanisms further reduce overall error rates by removing mispaired or damaged bases (7). Although the wide range of DNA repair mechanisms available to all cells can efficiently detect and remove a myriad of lesions from the DNA template, some forms of lesions persist and risk the survival of the cell because an unre-

*To whom correspondence should be addressed. Tel: +49 931866685; Email: christian.janzen@uni-wuerzburg.de
Correspondence may also be addressed to Richard McCulloch. Tel: +44 1413305946; Email: Richard.McCulloch@glasgow.ac.uk
†The authors wish it to be known that, in their opinion, the first two authors should be regarded as Joint First Authors.
Present address: Andrea Zurita Leal, Facultad de Ciencias de la Salud, Universidad Técnica de Ambato, Ambato, Ecuador.

paired lesion can lead to replication fork stalling and, potentially, death (8,9). Translesion synthesis (TLS) circumvents this problem (7), using TLS Pols to insert nucleotides in the new DNA strand and thereby bypassing a lesion in the template DNA strand. Recruitment of TLS Pols to damaged DNA is mediated by the proliferating cell nuclear antigen, PCNA (10). The homotrimeric PCNA complex encircles DNA and interacts with replicative DNA Pols, increasing their processivity (11). PCNA also interacts with TLS Pols through a PIP box motif (12). Indeed, it has been suggested that at least some TLS Pols form a multi-protein complex at stalled replication forks (13). Replication fork stalling also causes a prolongation of single-stranded DNA, which is recognized by the replication protein A (RPA) heterotrimer. RPA binding triggers mono-ubiquitination of PCNA by the RAD18/RAD6 complex (14), which facilitates the exchange of replicative polymerases with TLS polymerases and, thus, the bypass of a DNA lesion during replication.

Very little is known about TLS activity in *Trypanosoma brucei*, the causative agent of African Sleeping Sickness in humans and the devastating animal disease *Nagana* in sub-Saharan Africa. The only functional study to date described two primase-polymerase-like proteins called PPL1 and PPL2 (15). TLS activity of both polymerases was confirmed by their ability to insert nucleotides opposite thymine dimers in DNA templates *in vitro*. Moreover, depletion of PPL2 causes a severe cell cycle defect after most nuclear DNA synthesis is complete and activation of the DNA damage response (15). What endogenous feature(s) of the nuclear *T. brucei* genome PPL2 acts upon is unknown, though the TLS Pol was very recently shown to be a component of telomere-binding protein complexes in trypanosomes (16). Telomere-associated proteins are of particular interest in *T. brucei*. Besides their function in telomere maintenance, they are involved in one of the most important strategies used by pathogens to evade the vertebrate host immune response: antigenic variation (reviewed in (17)). In *T. brucei*, antigenic variation is mediated by a periodic exchange of a protective coat composed of variant surface glycoprotein (VSG) (18). There are >2000 VSG genes or pseudogenes in the *T. brucei* genome (19,20) but at any given time only a single VSG gene is expressed from one of ∼15 specialized loci, the so-called bloodstream VSG expression sites (BES) (21). BES are always located adjacent to telomeres and switching of the expressed VSG can occur by events that change which of the BES is singularly transcribed, or by recombination reactions that replace the BES VSG with a silent gene (22). Several telomere-associated proteins are known to be involved in the transcriptional control mechanisms that ensure only a single BES is transcribed, and to affect VSG recombination (17). For example, repressor activator protein 1 (RAP1) appears to be necessary for monoallelic expression of VSG genes because depletion of RAP1 partially de-represses all silent BES (23). Furthermore, it was shown that the telomere duplex DNA-binding factor TRF suppresses homologous recombination of VSG sequences into the active BES (24). The TRF interacting factor 2 (TIF2) also appears to be a negative regulator of VSG switching in collaboration with TRF, but by an additional mechanism that is independent from TRF association (25,26). Beyond such telomere-focused observations, recent work has shown that the actively transcribed BES is replicated early in S-phase, whereas all silent BES are replicated later (27). What factors dictate that only the transcribed BES is early replicating, and how the BES replication process relates to the rest of the genome, is unknown (28–30). Furthermore, accumulating evidence indicates that the active BES contains RNA–DNA hybrids (31,32), which can lead to DNA damage, and all BES are prone to lesions (33), but whether these observations relate to specific aspects of BES replication is unknown.

Since the exact mechanisms of BES monoallelic transcriptional control and potential targeting of recombination events in the BES remain elusive, we were intrigued to find that, in addition to PPL2, a further putative *T. brucei* TLS Pol, which we now refer to as TbPolIE, is a telomere-associated protein, since it could be purified with a telomeric repeat-containing oligonucleotide and by co-immunoprecipitation with TRF (16). Here, we show that TbPolIE is closely related to four mitochondrial-targeted DNA Pols but displays pronounced localization to the periphery of the nucleus in *T. brucei* mammal-infective cells, and that RNAi-mediated depletion of TbPolIE results in slowed growth without a specific cell cycle arrest, accumulation of DNA damage and chromosome segregation defects. We also document substantial deregulation of telomeric VSG genes after TbPolIE depletion, which suggests at least one TLS DNA Pol can contribute to antigenic variation.

MATERIALS AND METHODS

Sequence analysis

T. brucei, L. major and *T. cruzi* gene and protein sequences were retrieved from TriTrypDB version 33 (http://tritrypdb.org/tritrypdb/). Multiple alignment sequence analysis in Figure 1 was conducted using ClustalW and PolIErotein domain analysis was performed using InterPro 64.0 (https://www.ebi.ac.uk/interpro/) and Pfam 31.0 (http://pfam.xfam.org/). PolA domain-containing proteins were identified across the eukaryotic domain and in bacteria by BlastP (https://blast.ncbi.nlm.nih.gov/Blast.cgi?PROGRAM=blastp, default parameters, nr protein database), with the *T. brucei* (TREU927) sequence Tb92711.5550 as query. The eukaryotic species examined, NCBI taxonomy identifiers and their phylogenetic supergroups, were as follows: Opisthokonta (*Bos Taurus[9913], Homo sapiens [9606], Caenorhabditis elegans [6239], Drosophila melanogaster [7227], Hydra vulgaris [6087], Saccharomyces cerevisiae [4932]*); Amoebozoa (*Dictyostelium discoideum [352472]*); Viridiplantae (*Oryza sativa [39947], Arabidopsis thaliana [3702]*); Diplomonadida (*Giardia intestinalis [5741]*), SAR (*Plasmodium falciparum [36329], Thalassiosira pseudonana [35128]*), Rhodophyta (*Chondrus crispus [2769]*); Euglenazoa (*Trypanosoma brucei brucei [185431], Trypanosoma cruzi [353153], Leishmania major [347515]*). Bacterial strains queried were *Escherichia coli BW25113 [679895], Staphylococcus aureus 04-02981 [70333], Vibrio cholerae HC-55C2 [991972]* and *Clostridioides difficile 630 [272563]*. The blast hits were manually curated to remove duplicates and isoforms, leaving a single

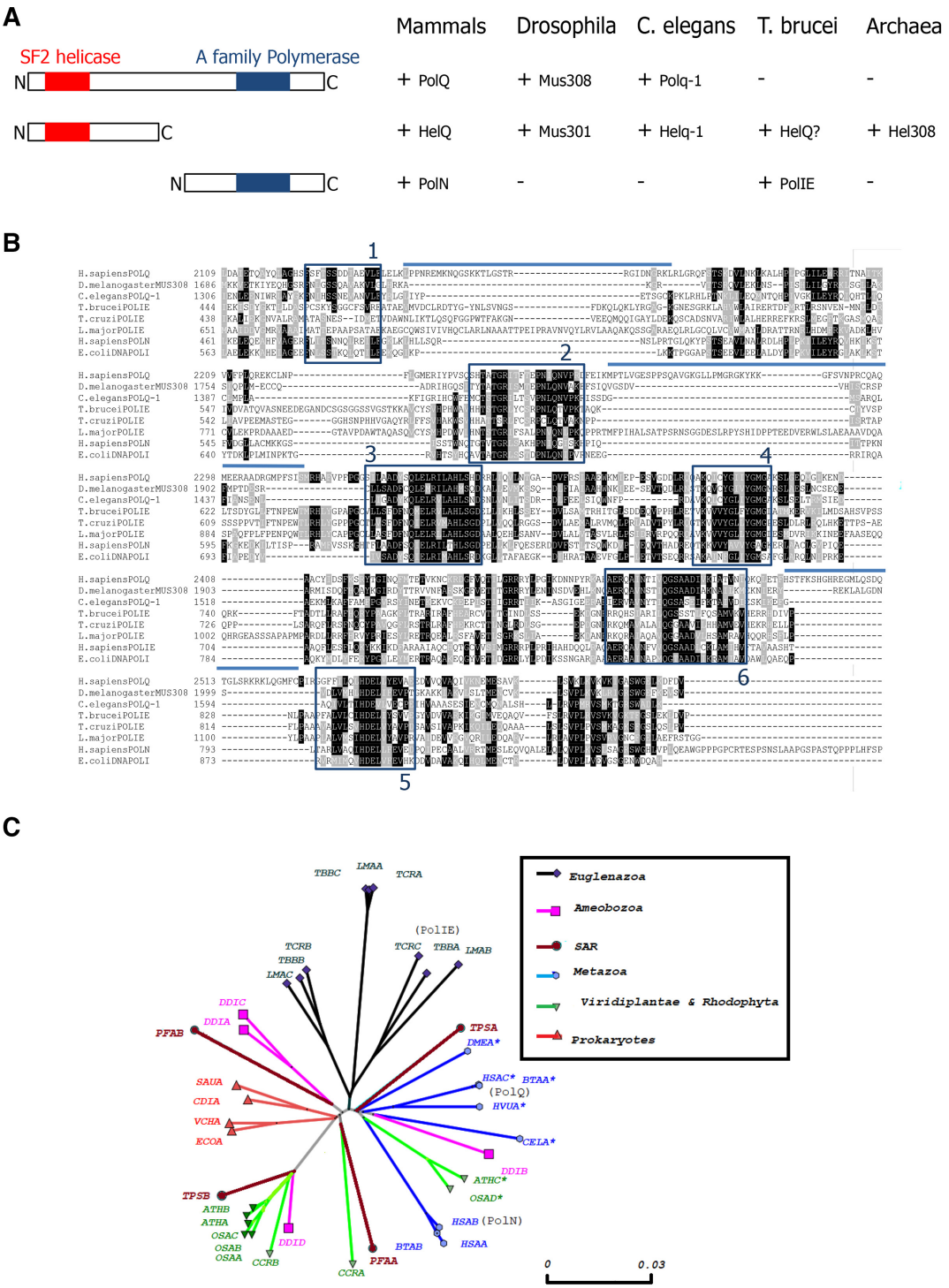

Figure 1. DNA Polymerase Q-related proteins in *Trypanosoma brucei*, selected multicellular eukaryotes and archaea. (**A**) Schematic representation of the distribution of conserved SNF2 helicase (red) and family A (blue) polymerase (Pol) domains found in homologous proteins described in mammals, *Drosophila melanogaster*, *Caenorhabditis elegans*, *T. brucei* and archaea (protein names are provided). (**B**) Sequence alignment of the Pol domain found in *H. sapiens* PolQ and PolN, *D. melanogaster,* Mus308, *C. elegans* Polq-1, *Escherichia coli* PolI and the predicted sequences of PolIE from *T. brucei*, *T. cruzi* and *Leishmania major*. Boxes 1–6 show conserved family A Pol motifs, and lines illustrate inserts associated with lesion bypass activity of PolQ. (**C**) A phylogenetic tree depicting the relationship between TbPolIE (TbbA) and identifiable PolA family DNA Pols in eukaryotes and bacteria; the insert explains colour coding of the tree branches based on eukaryotic supergroups or prokaryotes, protein annotations are described in Table 1 (SAR denotes the eukaryotic supergroup Stramenopiles, Alveolates and Rhizaria). (*) denotes proteins with both Pol and helicase domains, and species are denoted as follows: Ath, *Arabidopsis thaliana*; Bta, *Bos Taurus*; Ccr, *Chondrus crispus*, Cdi, *Clostridioides difficile*; Cel, *Caenorhabditis elegans*; Ddi, *Dictyostelium discoideum*; Dme, *Drosophila melanogaster*; Eco, *Escherichia coli*; Hsa, *Homo sapiens*; HvuA, *Hydra vulgaris*; Lma, *Leishmania major*; OsaA, *Oryza sativa*; Pfa, *Plasmodium falciparum*; Sau, *Staphylococcus aureus*; Tbb, *Trypanosoma brucei brucei*; Tcr, *Trypanosoma cruzi*; TpsA, *Thalassiosira pseudonana*; Vch, *Vibrio cholerae*.

canonical entry for each hit. A parallel blastp search was performed using the sequences of Tb927.8.3550 was performed. Identifiers present in this hit set and the canonical PolA set were flagged as potentially containing both the PolA and helicaser domains. Protein sequences and IDs recovered were as shown in Table 1.

To evaluate relationships amongst the above PolA domain-containing proteins, the PolA domain for each was extracted and the sequences aligned using the following web-based programs; all using default parameters:

CLUSTAL Omega (https://www.ebi.ac.uk/Tools/msa/clustalo/)
Muscle (https://www.ebi.ac.uk/Tools/msa/muscle/)
Kalign (https://www.ebi.ac.uk/Tools/msa/kalign/)
Mafft (https://www.ebi.ac.uk/Tools/msa/mafft/)
T_coffee (http://tcoffee.crg.cat/apps/tcoffee/do:regular)
T_coffee:Expresso (http://tcoffee.crg.cat/apps/tcoffee/do:expresso)

From these alignments, a consensus alignment was derived using t-COFFEE (http://tcoffee.crg.cat/apps/tcoffee/do:combine). Columns with an occupancy <15%, or overall quality <3 were removed.

Analysis of the consensus alignment was performed using SplitsTree5 5.0.0_alpha (34). The original input consisted of 38 taxa and 38 Protein character sequences of length 1406. The Hamming Distances method (35) was used (default options) so as to obtain a 38 × 38 distance matrix. The Neighbor Net method (36) was used (default options) so as to obtain 127 splits, cyclic. The Neighbor Joining method (37) was used so as to obtain one tree. The PCo A2 D method (38) was used (default options) so as to obtain 38 nodes and 0 edges. The Consensus Network method (39) was used (default options) so as to obtain 73 splits, compatible. The Splits Network Algorithm method (40) was used (default options) so as to obtain a splits network with 74 nodes and 73 edges. The Splits Network Algorithm method (40) was used (default options) so as to obtain a splits network with 548 nodes and 967 edges.

Maintenance of cell cultures

Lister 427 (WT) bloodstream form (BSF) cells were grown in HMI-9 (Gibco®) (Hirumi and Hirumi, 1989), supplemented with 20% (v/v) heat inactivated fetal bovine serum (FBS; Sigma Aldrich) and 1% penicillin-streptomycin solution (stock at 10 000 U/ml) (Gibco®). In the case of the 2T1 cell line, the cells were grown in HMI-11 thymidine-free media, consisting of Iscove's modified Dulbecco's medium (IMDM) (Gibco®), 10% (v/v) of FBS (Gibco®,tetracycline free), 1% of penicillin-streptomycin solution (10 000 U/ml) (Gibco®). For the RNAi cell lines used in EdU replication assays, the cells were grown in HMI-11 thymidine free media, consisting of Iscove's modified Dulbecco's medium (IMDM) (Gibco®), 10% (v/v) of FBS (Gibco®, tetracycline free), 1% of penicillin–streptomycin solution (10 000 U/ml; Gibco®), 4% (v/v) of HMI-9 mix (0.05 mM of bathocuproine disulphonic acid, 1 mM of sodium pyruvate, and 1.5 mM of L-cysteine, 1 mM of hypoxanthine and 0.0014% of 2-mercaptoethanol (Sigma Aldrich)). For Lister 427 (WT), no drugs were added to the media. The selective drugs used for 2T1 cells were puromycin (0.2 μg/ml) and phleomycin (2.5 μg/ml), for RNAi cell lines phleomycin (2.5 μg/ml) and hygromycin (5 μg/ml) and for N50 (41) neomycin (2.5 μg/ml). The tagged cells were grown in medium with 10 μg/ml blasticidin.

Western blot

Western botting was performed according standard protocols, using ∼2 × 10^6 parasites. TbPolIE-12myc was detected using mouse anti-myc clone 4A6 antibody at 1:7000 (Millipore). The detection of Ef1α (loading control), was performed with the mouse anti-Ef1α clone CBP-KK1 antibody at 1:25 000 (Millipore). Both antibodies were used in combination with the goat anti-mouse IgG (H+L) horseradish peroxidase conjugate at 1:3000 (Life Technologies). While the damage accumulation marker γH2A (42) was detected using rabbit anti-γH2A at 1:10 000 in combination with goat anti-rabbit IgG (H+L) horseradish peroxidase conjugate at 1:3000 (Life Technologies). To analyse VSG expression, cell lysates of ∼2 × 10^6 cells were separated by SDS-PAGE and transferred to a PVDF membrane. VSGs were detected using polyclonal antibodies from rabbits immunized with VSG2, VSG3, VSG6 or VSG13 (gift from Markus Engstler, University Wuerzburg). Signal intensity was normalized using a monoclonal antibody L13D6 specific for a paraflagellar rod protein (Gift from Keith Gull, University of Oxford). IRDye680- or IRDye800-conjugated secondary antibodies were used in combination with an Odyssey infrared scanner (LI-COR).

TbPolIE endogenous epitope tagging

TbPolIE gene was modified *in situ* in *T. brucei* BSF cells, strain Lister 427, in order to express the protein as a C-terminal fusion of the myc epitope. To accomplish this, the protein was C-terminal tagged with 12 tandem repeats of the myc epitope using the $pNAT^{12myc}$ BSD vector (43). The 3′ end of TbPolIE ORF, with the exclusion of the stop-codon, was PCR-amplified using the following primers Fw-gcatgagctcacgagttgctcattaagcac and Rv-gcattctagaaggaacatcaagtttctcga. The forward primer contained a SacI restriction site and the reverse primer contained a XbaI restriction site, facilitating the cloning of the fragment into the vector. The resulting vector was linearized prior to transfection using PstI. The transformants were selected using 10 μg/ml blasticidin.

TbPolIE cellular localization

TbPolIE cellular localization was tested before and after genotoxic stress. Two cultures containing 2 × 10^5 cells were grown in the presence of 10 μg/ml basticidin, one culture was treated with 0.003% MMS. After 18 h, 2 × 10^6 parasites were harvested by centrifugation (405 × g) and washed with PBS. Next, 25 μl of the cell suspension was loaded to 12 multi-well glass slide, pre-treated with poly-L-lysine and allowed to settle for 5 min. The cells were fixed with 4% paraformaldehyde for 5 min and permeabilized with 0.2% Triton X-100 (Promega) in PBS for 10 min. Next, 100

Table 1. PolA DNA Pols used in phylogenetic analysis; shortened protein names are as detailed in Figure 1C (* denotes proteins that contained both PolA and helicase domains)

Protein	Accession no.	Database annotation [organism]
AthA	AAG50942.1	DNA polymerase A family protein, putative [*Arabidopsis thaliana*]
AthB	NP_188690.3	Polymerase gamma 1 [*Arabidopsis thaliana*]
AthC*	NP_001078482.1	MUS308 and mammalian DNA polymerase-like protein [*Arabidopsis thaliana*]
AthD	NP_001321058.1	polymerase gamma 2 [*Arabidopsis thaliana*]
BtaA*	XP_002684835.1	DNA polymerase theta isoform X1 [*Bos taurus*]
BtaB	XP_002688485.4	DNA polymerase nu [*Bos taurus*]
CcrA	XP_005717334.1	Unnamed protein product [*Chondrus crispus*]
CcrB	XP_005719396.1	DNA polymerase type I with a mitochondrial signal peptide [*Chondrus crispus*]
CdiA	AJP10819.1	DNA polymerase I (POLI) [*Clostridioides difficile* 630]
CelA*	NP_001367994.1	DNA polymerase theta [*Caenorhabditis elegans*]
DdiA	XP_640197.1	Hypothetical protein DDB_G0282679 [*Dictyostelium discoideum* AX4]
DdiB	XP_642487.1	Hypothetical protein DDB_G0277751 [*Dictyostelium discoideum* AX4]
DdiC	XP_644204.1	Hypothetical protein DDB_G0274421 [*Dictyostelium discoideum* AX4]
DdiD	XP_647557.1	Mitochondrial DNA polymerase A [*Dictyostelium discoideum* AX4]
DmeA*	NP_524333.1	DNA polymerase theta [*Drosophila melanogaster*]
EcoA	AIN34166.1	Fused DNA polymerase I 5′-_3′ polymerase/3′-_5′ exonuclease/5′-_3′ exonuclease [*Escherichia coli* BW25113]
HsaA	BAD18421.1	Unnamed protein product [*Homo sapiens*]
HsaB	NP_861524.2	DNA polymerase nu [*Homo sapiens*]
HsaC*	NP_955452.3	DNA polymerase theta [*Homo sapiens*]
HvuA*	XP_012557649.1	PREDICTED: DNA polymerase theta-like isoform X2 [*Hydra vulgaris*]
LmaA	XP_001687691.1	Putative mitochondrial DNA polymerase I protein C [*Leishmania major* strain Friedlin]
LmaB	XP_001683604.1	Putative DNA polymerase theta [*Leishmania major* strain Friedlin]
LmaC	XP_001686222.1	Putative mitochondrial DNA polymerase I protein A [*Leishmania major* strain Friedlin]
OsaA	XP_015636766.1]	DNA polymerase I A, chloroplastic-like isoform X1 [*Oryza sativa* Japonica Group
OsaB	XP_015650231.1	DNA polymerase I B, mitochondrial isoform X3 [*Oryza sativa* Japonica Group]
OsaC	XP_015650956.1	DNA polymerase I A, chloroplastic [*Oryza sativa* Japonica Group]
OsaD*	XP_015619406.1	Helicase and polymerase-containing protein TEBICHI [*Oryza sativa* Japonica Group]
PfaA	XP_966236.1	DNA polymerase 1, putative [*Plasmodium falciparum* 3D7]
PfaB	XP_001348285.1	plastid replication-repair enzyme [*Plasmodium falciparum* 3D7]
SauA	ADC37860.1	DNA polymerase I [*Staphylococcus aureus* 04-02981]
TbbA	XP_828630.1	DNA polymerase theta, putative [*Trypanosoma brucei brucei* TREU927]
TbbB	XP_844445.1	Mitochondrial DNA polymerase I protein A, putative [*Trypanosoma brucei brucei* TREU927]
TbbC	XP_846022.1	Mitochondrial DNA polymerase I protein C [*Trypanosoma brucei brucei* TREU927]
TcrA	XP_810416.1	Mitochondrial DNA polymerase I protein C [*Trypanosoma cruzi* strain CL Brener]
TcrB	XP_817509.1	Mitochondrial DNA polymerase I protein A [*Trypanosoma cruzi* strain CL Brener]
TcrC	XP_818250.1	DNA polymerase theta (polymerase domain only) [*Trypanosoma cruzi* strain CL Brener]
TpsA	XP_002291263.1	DNA polymerase [*Thalassiosira pseudonana* CCMP1335]
TpsB	XP_002294547.1	Hypothetical protein THAPSDRAFT_270013 [*Thalassiosira pseudonana* CCMP1335]
VchA	EKL09444.1	DNA polymerase I family protein [*Vibrio cholerae* HC-55C2]

mM glycine was added for 20 min and washed twice with PBS for 5 min. Afterwards, the cells were incubated with 1% BSA/0.2% Tween-20 in PBS for 1 h. The mouse anti-myc 4A6 Alexa Fluor® 488 conjugated antiserum diluted 1:500 in 1% BSA/0.2% Tween in PBS was applied for 1hr, followed by two washes with 3% BSA in PBS. After, the Fluoromount G containing DAPI mounting medium was added; the slide was covered with a coverslip and sealed with regular nail varnish. The images were captured in the Deltavision RT deconvolution fluorescence microscope, the 1.4/63× lens was used. Z-stacks of 6 μm (30 sections, 0.2 μm thickness each) were acquired using SoftWoRx Suite 2.0 (Applied Precision, GE). High resolution images were captured on an Elyra PS.1 super resolution microscope (Zeiss) using the 1.4/63× lens. The images were acquired using the ZEN Black Edition Imaging software.

Construction of TbPolIE RNAi cell line

A fragment of the TbPolIE gene was PCR amplified from *T. brucei* TREU 927, using primers PolIEC1, PolIEC4, PolIEC9 (sequences upon request), incorporating the attB1 and attB2 sites. The fragment was cloned into the pPGL2084 vector (44) in a BP recombinase reaction, using the Gateway® BP clonase® II Enzyme mix Kit (Life Technologies), following the manufacturer's instructions. The final vector was linearized with AscI and transfected into the genetically modified Lister 427 strain, 2T1 (43). The transformants were selected with 5 μg/ml hygromycin, in the presence of 2.5 μg/ml phleomycin.

Survival assay

TbPolIE RNAi cell line was cultured in tetracycline (Tet) free medium containing phleomycin and hygromycin. Parasites were dilute into two cultures of 1×10^4 cells/ml, one containing 1 μg/ml tetracyclin (Tet+) to induce the RNAi-mediated depletion of the gene. The population density was assessed every 24 for a period of 3 days, using the Neubauer haemocytometer. The cells survival was also tested after the exposure to genotoxic stress. The cells were prepared as described above. Both flasks were mixed and 1 ml of each culture aliquoted to a 24-well plate. The appropriate concentration (0%, 0.001%, 0.002%, 0.003%) of MMS was added to each well of Tet– and Tet+ cells, assessing the population density every 24 h. In the case of UV exposure the Tet– and

Tet+ cells were UV irradiated (0, 500, 750, 1000 and 1500 J/m^2) 24 h post-induction using a Stratagene Stratalinker UV Crosslinker 2400.

Damage accumulation assay

Two cultures containing 2 × 10^4 TbPolIE RNAi cells were grown in the absence and presence of 1 μg/ml of tetracycline. After 24, 48 and 72 h, 2 × 10^6 parasites were harvested by centrifugation (405 × g) and washed with 1× PBS. The cells were prepared for western blot and immunofluorescence as described above. For both approaches anti-γH2A antibody, which recognizes Thr130 phosphorylated histone H2A, was diluted to a concentration of 1:1000 and detected with α-rabbit HRP conjugate (1:3000) for western blot and Alexa Fluor® 594 α-rabbit (1:1000) for immunofluorescence analysis.

EdU incorporation assay

TbPolIE RNAi cells were incubated with 150 μM of 5-ethynil-2′-deoxyuridine (EdU; Life Technologies) for 4 h at 37°C with 5% CO_2. The cells were then harvested by centrifugation at 1000 × g for 5 min and washed with 1× PBS. The pellet was re-suspended in 20 μl of 1× PBS and the cell suspension was pipetted onto a 12 well slide, pre-treated with poly-L-lysine, and left to settle for 5 min. The supernatant was removed and 25 μl of 4% paraformaldehyde was added and left for 4 min, followed by a wash with 3% BSA in 1× PBS. The cells were permeabilized by adding 20 μl of 0.2% Triton X-100 (Promega) in 1× PBS for 10 min at room temperature. The wells were washed twice with 3% BSA in 1× PBS. The supernatant was removed and 25 μl of the Click-iT® (Life Technologies) reaction, containing 21.25 μl of 1× Reaction Buffer, 1 μl of $CuSO_4$, 0.25 μl Alexa Fluor® 555 Azide and 2.5 μl of 1× Reaction Buffer, was added for 1 h at room temperature. The solution was removed and the cells were washed 6 times with 3% BSA in 1× PBS. The Fluoromount G containing DAPI mounting medium was added and the slide was covered with a coverslip and sealed. In the case of a double labeling detection, EdU signal and phosphorylated γH2A signal, the sample was incubated first with the Click-iT® reaction, followed by 1 h incubation with 1% BSA/0.2% Tween-20 in 1× PBS. Afterwards, anti-γH2A antibody diluted 1:1000 was added for 1 h and detected with Alexa Fluor® 594 α- rabbit diluted 1:1000. The images were captured using a Zeiss Axioskop 2 fluorescent microscope (63×/1.4 oil objective). The images were acquired using the ZEN software package (Zeiss; http://www.zeiss.com/corporate/en_de/home.html).

Measurement of fluorescence intensity

For the intensity analysis the software Fiji (ImageJ) was used to convert images to grayscale and to subtract the background. A circle of 2.1 × 2.1 pixel region of interest (ROI) was drawn around the cell, obtaining the density (area and the mean gray value) and mean fluorescence value of each cell. For each image, a region with no fluorescence was selected, which corresponds to the background control. The fluorescence intensity was obtained by calculating the corrected total cell fluorescence (CTCF) using the following formula:

$$\text{CTCF} = \text{Integrated density} - (\text{Area of selected cell} \times \text{mean fluorescence of background readings})$$

Fluorescence *in situ* hybridization (FISH)

Approximately 5 × 10^6 cells were harvested by centrifugation at 405 × g for 10 min and washed in 1× PBS at 660 × g for 3 min. The supernatant was removed and the pellet re-suspended in 4% formaldehyde in 1× PBS for 20 min at room temperature. The cells were washed and re-suspended in 65 μl of 1× PBS and spread onto a pre-treated poly-L-lysine (Sigma Aldrich) slide and left to settle for 20 min. The supernatant was removed and the cells permeabilized with 0.1% Triton X-100 in 1× PBS for 3 min. The cells were washed and dehydrated with pre-chilled ethanol in ascending concentration (70–90–100%) for 5 min each concentration. The slide was left to dry. In the meantime, 10 μl of the telomere probe (TTAGGG; Thermo Fisher) was added into 60 μl of hybridization solution (50% Formamide, 10% Dextran, 2× SSPE buffer [1× SSPE: 0.18 M NaCl, 10 mM NaH_2P0_4, 1 mM EDTA, pH 7.7: use buffer at pH 7.9]) and heated at 85°C in a water bath for 7 min. Once the slide was completely dry the hybridization solution containing the probe was added. The slide was covered with a plastic coverslip and incubated at 95°C for 5 min (water bath), followed by 16 h incubation at 37°C. Then, the coverslip was removed and the slide was washed for 30 min with 2× SSC (Thermo Fisher)/50% Formamide solution at 37°C, 60 min with 0.2× SCC at 50°C and a final wash with 4× SSC at room temperature for 10 min. The slide was finally mounted in Fluoromount G containing DAPI and sealed with nail varnish.

Cell viability assay

Approximately 1 × 10^6 cells were harvested and washed twice with 1 ml trypanosome dilution buffer (TDB; 5 mM KCl, 80 mM NaCl, 1 mM $MgSO_4$, 20 mM Na_2PO_4, 2 mM NaH_2PO_4, 20 mM glucose, pH 7.4) (1500 × g, 4°C, 10 min). The supernatant was discarded and the pellet was taken up in 400 μl TDB. Propidium iodide was added in a final concentration of 2.5 μg/ml to the resuspended pellet and incubated for 10 min on ice. Analysis of the dyed cells was performed with a BD FacsCalibur. For the analysis of dead cells, WT cells without puromycin resistance were incubated overnight with a final concentration of 1 μg/ml puromycin.

Cell cycle analysis with propidium iodide

2 × 10^7 cells harvested and washed with 1 ml PBS (1500 × g, 4°C, 10 min). The cell pellet was resuspended in 2 ml ice-cold PBS/2 mM EDTA and fixed by the dropwise addition of 2.5 ml ice-cold EtOH. After 1 h of incubation at 4°C, the cells were washed with 1 ml PBS (1500 × g, 4°C, 10 min) and the pellet resuspended in 1 ml PBS. 10 μg RNaseA and propidium iodide in a final concentration of 10 μg/ml were added to the suspension. After inverting of the sample three time, the cell suspension was incubated for 30 min at 37°C.

Cells were stored at 4°C before analysis with a BD FACSCalibur and CellQuest Pro 6.9.

Isolation of soluble VSG for mass spectrometry analysis

Approximately 4 × 10^7 cells were precooled for 10 min on ice and then harvested with 1500 × g for 10 min at 4°C. The cell pellet was resuspended in 45 μl 10 mM sodium phosphate buffer with additional protease inhibitors (leupeptin, PMSF and TLCK). The suspension was incubated for 5 min at 37°C and then cooled down for 2 min on ice. The cells were sedimented (14 000 g, 4°C, 5 min) and only the supernatant transferred to a new reaction tube. 15 μl of 4× NuPage® Buffer (Invitrogen) supplemented with 400 mM DTT was added to the suspension and incubated at 70°C for 10 min. The cell suspension was stored at –20°C until the shipping to Falk Butter (IMB Mainz) for mass spectrometry analysis. The experiment was conducted in quadruplicate. The samples were loaded into a 10% NuPage NOVEX gel and run in 1× MES (Thermo) at 180 V for 10 min. The gel was fixated and stained with Coomassie (Sigma). The gel lanes were sliced, destained in 50% EtOH/25 mM ABC (ammonium bicarbonate) pH 8.0, reduced in 10 mM DTT (Sigma) for 30 min at 56°C and subsequently alkylated with 55 mM iodoacetamide (Sigma) for 30 min at RT in the darkd. Proteins were digested with MS-grade trypsin (Sigma) overnight at 37°C and tryptic peptides desalted and stored on StageTips. For MS analysis, peptides were separated on an in-house packed Reprosil C18-AQ 1.9 μm resin (Dr. Maisch GmbH) capillary (New Objective) with an optimized 75 min gradient from 2% to 40% ACN (with 0.1% formic acid) prepared with an Easy-nLC 1000 system (Thermo). The packed capillary was mounted in a column oven (Sonation) and sprayed peptides continuously into a Q Exactive Plus mass spectrometer (Thermo) operated with a top10 data-dependent acquisition mode. Spray voltage was set between 1.8 and 2.4 kV. The MS raw files were processed with MaxQuant (version 1.5.2.8) using standard settings with additionally activated LFQ quantitation and match between runs option. For the search, a concatenated database of TriTrypDB-8.1_TbruceiLister427_AnnotatedProteins.fasta (8833 entries), TriTrypDB-8.1_TbruceiTREU927_AnnotatedProteins.fasta (11 567 entries) and the Lister427 VSG gene fasta (GAM Cross) translated in three reading frames vsgs_tb427_cds.out.fasta (86 764 entries) was used. For data analysis, all protein groups with less than two peptides (one unique + one razor) and all protein groups not containing a VSG annotation as primary entry were removed. For the remaining Lister427 VSG proteins from the VSG gene fasta, the mean LFQ expression value of the quadruplicates was calculated and plotted as VSG abundance in R.

RESULTS

T. brucei encodes separate DNA polymerase and helicase proteins related to the two domains found in eukaryotic PolQ (theta)

Eukaryotic cells express a range of factors related to DNA PolQ (theta), a protein that possesses both a C-terminal family A DNA Pol domain and an N-terminal super family 2 helicase domain (Figure 1A, (45)). PolQ has been implicated in a wide range of cell functions, including lesion bypass (46–48), DNA break repair by microhomology-mediated recombination (including during the repair of stalled DNA replication) (49–52), and initiation of DNA replication (53). In contrast, where organisms express related proteins possessing just the PolQ-like DNA Pol domain (PolN in mammals) or helicase domain (HelQ in mammals), their functions are less clearly understood (45). PolIN-like proteins have to date only been described in metazoans, where TLS activities (54–56) and roles in interstrand cross link and recombination repair (57–59) have been detailed, whereas HelQ-like proteins have been investigated in multicellular eukaryotes and archaea (Figure 1A) (45,60–63). In kinetoplastids, a DNA Pol has been annotated as PolQ-related (for instance, Tb927.11.5550: Pol theta polymerase (64)), but in all these organisms the protein contains no detectable helicase domain, since a PolQ- or HelQ-related helicase is encoded from unlinked, syntenic genes (Figure 1A). Structurally, these kinetoplast Pols therefore appear more similar to PolN proteins in metazoans, though sequence alignment of the Pol from *T. brucei*, *T. cruzi* and *L. major* do not readily reveal greater sequence homology between the parasite proteins and human PolQ or PolIN (Figure 1B). In all cases, six conserved Pol domains could be predicted, consistent with Pol activity, as seen in the purified protein from *L. infantum* (there called PolQ (64)). However, sequence insertions between some of the Pol domains, which have been shown to underlie the lesion bypass activity of human PolQ (47), are much more marked in the *L. major* Pol than in the orthologues from *T. brucei* or *T. cruzi* (Figure 1). Whether this might mean alteration in TLS functions of the *Trypanosoma* proteins relative to the ability of the *L. infantum* Pol to bypass 8oxoG, abasic sites and thymine glycol lesions *in vitro* is unclear (64).

To attempt to understand how the kinetoplastid Pols might have arisen during evolution, and thereby gain insight into their potential function, we identified PolA-family DNA Pols in 11 species spanning the supergroups comprising the eukaryotic domain (Table 1). We then compared all the proteins identified with each other, as well as with better characterized PolQs and PolNs in humans, *Caenorhabditis elegans*, *Drosophila melanogaster* and with PolIs in four species of bacteria. To do this, we generated a consensus alignment of the isolated PolA domains after performing six different alignments with distinct programmes (Supplementary Figure S1) and, from the consensus, drew a phylogenetic tree (Figure 1C). These data revealed three things. First, PolA-like proteins that group closely with bacterial PolI are widespread in eukaryotes, most likely providing mitochondrial, chloroplast or plastid functions (such as in *Plasmodium* (65)). Second, DNA Pols that group with PolQ or PolN are absent from numerous species across the eukaryotic domain, including *Saccharomyces cerevisiae*, *Giardia intestinalis*, *Plasmodium falciparum* and *Chondrus crispus.* Consistent with previous analysis (59), PolQ-like proteins were detected in a larger number of species than PolIN-like proteins, though proteins containing only Pol domains and grouping with PolQ are not limited to metazoans, as they were detected in

Dictyostelium discoideum (an amoeba) and *Thalassiosira pseudonana* (a diatom). Third, and surprisingly, the trypanosomatid DNA Pols annotated in the genome database as being PolQ-like did not group with PolQ- or PolNlike proteins found in other eukaryotes, but instead formed a robust grouping with mitochondrial-targeted enzymes that were previously detected in genome searches with bacterial PolI and, hence, have been considered PolI-like. To date, four such PolI-like enzymes have been described in *T. brucei* (66), and each (named TbPolIA-D; for simplicity, only two are shown in Figure 1C) have been shown to localize to the parasite mitochondrion, where they act to maintain the mitochondrial genome network, termed the kinetoplast (67). Though the *T. brucei* protein encoded by Tb927.11.5550 is clearly nuclear (see below), these data suggest a family of PolA DNA Pols genes arose and diversified in the kinetoplastids lineage, without clear evidence for the ancestral gene being bacterial PolI-like or PolQ/N-like. Given this, we have chosen to refer to the *T. brucei* nuclear protein as TbPolIE, reflecting its identity as one of five putative DNA Pol paralogues with unclear evolutionary ancestry.

Super-resolution imaging reveals subnuclear localization of TbPolIE

Identification of TbPolIE as a telomere-associated protein (68) demonstrates that, unlike TbPoIIA-D, it is nuclear. To further explore its potential function, localization of TbPolIE was assessed by immunofluorescence imaging using a cell line generated to express the protein PolIE as a fusion to 12 C-terminal copies of the myc epitope (TbPolIE-12myc; Figure 2). Western blotting revealed expression of a myc-tagged protein of the expected size (Supplementary Figure S2A). Intracellular localization was examined with and without growth of the cells in the presence of the alkylating agent methyl methanesulfonate (MMS, 0.003%) for 18 h. In both conditions, all anti-myc signal was found in the nucleus (Supplementary Figure S2B, C), and in the absence of MMS treatment, confocal images suggested localization of the protein in discrete subnuclear puncta (Supplementary Figure S2B). Structure illuminated super-resolution imaging revealed multiple puncta, with two relatively intense puncta present at the nuclear periphery in all cells (Figure 2). After growth in MMS, anti-myc signal was more dispersed throughout the nucleoplasm, perhaps suggesting redistribution of TbPolIE-12myc in the presence of damage (Figure 2). What features of the nuclear genome or nucleus are predominantly localized in the two regions of the nuclear periphery is unclear. However, fluorescent imaging of both TbPolIE-12myc and Thr130-phosphorylated histone H2A (yH2A), did not reveal extensive overlap of the two signals with or without MMS treatment (Supplementary Figure S3), suggesting TbPolIE is not associated with the small numbers of relatively discrete lesions marked by yH2A in WT cells (31,69), nor is it recruited to all the damage generated by MMS.

TbPolIE is important for growth of bloodstream form *T. brucei*

To learn more about the function of TbPolIE in trypanosomes, we used tetracycline-inducible RNAi to deplete the protein in BSF cells (Figure 3). Stagnation of growth was observed 24 h post induction of RNAi (Figure 3A). To ask if this growth defect could be explained by cell cycle arrest, we used flow cytometry to analyse the DNA content of propidium iodide-stained parasite populations at several time points after induction (Figure 3B, left panel). Numbers of 1N (G1 phase) cells were found to decrease in abundance with time, without equivalent accumulation of either 1N-2N (S phase) or 2N (G2/M) cells, suggesting there was no arrest at an observable cell cycle stage (Figure 3B, right panel). In fact, we could observe a slight but significant decrease in S-phase cells. Loss of 1N cells was concomitant with increased numbers of cells with <1N DNA content, indicating that loss of TbPolIE led to cells that had lost nuclear genome content. To ask if growth arrest after RNAi might also reflect cell death, we determined how many unpermeabilized cells could take up and be stained with propidium iodide (Supplementary Figure S4). Forty-eight hours after RNAi induction, when growth was strongly affected and substantial loss of G1 cells was detected, only around 10% of cells were classified as 'dead' by this approach. Hence, it seems unlikely that stagnation of cell growth after TbPolIE loss is caused predominantly by cell death.

To ask if TbPolIE contributes to DNA repair, growth was evaluated before and after RNAi in the presence of MMS and after exposure to UV light (Supplementary Figure S5). In each case, the extent of growth impairment caused by addition of the genotoxic agents was slightly more pronounced after RNAi than before. Thus, although TbPolIE-12myc does not display extensive colocalization with yH2A signal after MMS exposure (Figure 2), it may contribute to the response to alkylation damage and the distinct lesions caused by UV. Whether the range of damage TbPolIE acts on overlaps with or is distinct from the orthologous protein in *L. infantum* is unclear, but LiPolIE is also implicated in tackling a range of lesions (64), perhaps suggesting a wide range of activities for kinetoplastid PolIEs.

Analysis of aberrant cells 48–72 h post RNAi induction

To learn more about the effects of TbPolIE depletion, cells from 24–72 h after RNAi induction were stained with 4′,6-diamidino-2-phenylindole (DAPI), which allows visualization of the trypanosome nucleus (N) and the kinetoplast (K) (Figure 4). Depending on the stage of the cell cycle the N–K content of an individual will vary, because replication and segregation of the nucleus and kinetoplast differ in their timing (70). Cells displaying a 1N1K content are predominantly in G1, though some may have entered nuclear S (which can also be seen by an elongated K configuration and, perhaps, increased N staining). Cells with 1N2K configuration are predominantly in G2/M, and cells that have completed mitosis and are undergoing cytokinesis are 2N2K. Changes in the distribution of these configurations in mutants or after RNAi indicate altered cell cycle dynamics, and non-standard configurations have been detailed to arise after mutation or depletion of specific genes (71,72). In this experiment, RNAi was performed in cells in which TbPolIE-12myc was expressed from its own locus, allowing us to evaluate the effectiveness of the knockdown. Twenty

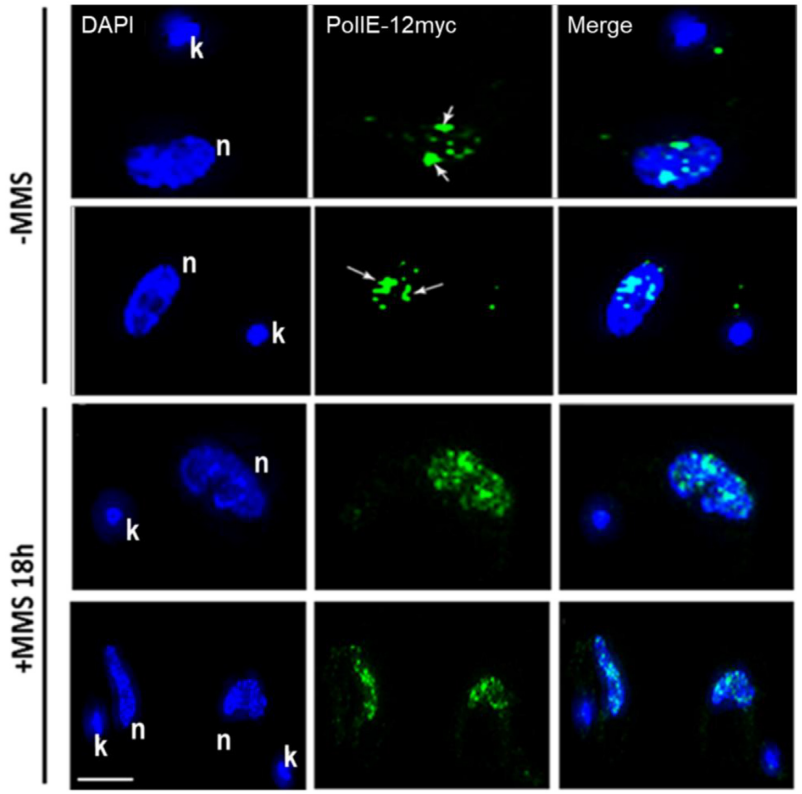

Figure 2. Subcellular localization of TbPolIE. Immunolocalization of TbPolIE-12myc in *T. brucei* BSF cells: left panels show DAPI staining of the nucleus (n) and kinetoplast (k), the middle panels show localization of TbPolIE-12myc using a conjugated Alexa Fluor® 488 anti-myc antibody, and the right panels are merged images of both signals. Images are shown of cells grown without damage (-MMS) or after growth for 18 h in the presence of 0.003% methyl methanesulphonate (+MMS 18 h). Arrows highlight two sites of significant TbPolIE-12myc signal seen at the periphery of the nucleus in all untreated cells. Images were captured on a Zeiss Elyra Super Resolution Microscope. Scale bar represents 2 μm.

four hours after depletion of TbPolIE, the DNA content distribution of the population and cell outline did not seem to be strongly affected, though a minor increase in the number of 1N2K cells, a small decrease in 2N2K cells and the appearance of cells with non-standard DNA configurations ('other') was apparent in light of the effects seen later. Forty-eight hours post RNAi induction a pronounced decrease in 1N1K cells and a further loss of 2N2K cells was clearly seen. In addition, though the numbers of 1N2K cells did not appear to increase further relative to 24 h, there was a very strong accumulation of cells with aberrant DNA content. At the same time, the cells had lost their typical trypomastigote shape. DNA content in the aberrant cells was hard to classify, but most cells had multiple kinetoplasts and abnormal, enlarged nuclei. These data suggest an initial, partial arrest in G2/M after loss of TbPolIE, which is then overridden and the cells progress to mitosis but cannot complete it accurately, explaining the reduction in 2N2K cells, accumulation of abnormal cells, and the strong decrease of 1N1K (G1) cells. Overall, the DAPI analysis also appears consistent with the flow cytometry (Figure 3). Surprisingly, the DAPI time course also revealed that the pronounced cell cycle perturbations seen 48 h after RNAi induction were somewhat transient phenotypes, since at 72 h the numbers of 1N1K cells increased and the numbers of aberrant cells decreased relative to 48 h (Figure 4B); in addition, it was possible to observe greater numbers of cells with more regular body shape (Figure 4A). The basis for this change is unclear, since western blot analysis indicated that levels of TbPolIE-12myc were reduced from 24 h after RNAi induction, and the protein was still undetectable at 72 h. Moreover, the apparent reversion was not associated with increased growth, as the RNAi cells still grew more slowly than uninduced controls at 72 h. Nonetheless, the shift from a severe to a less severe cell cycle perturbation from 48 to 72 h was mirrored in two other phenotypes we examined (see below).

TbPolIE loss is associated with aberrant cell morphology

As detailed above, RNAi depletion of TbPolIE resulted in significant changes in cell morphology, especially 48 h post induction. In order to evaluate these observations further, transmission electron microscopy (TEM) and scanning electron microscopy (SEM) were employed (Figure 5). TEM was performed in order to examine the ultrastructure of TbPolIE RNAi depleted cells relative to uninduced controls, facilitating the visualization of the nucleus, kinetoplast and flagellar pocket. SEM allowed visualization of the external architecture of BSF cells. Upon depletion of TbPolIE, clear alterations were observed in the internal morphology of the cell. Unlike in uninduced cells, the kinetoplast could not clearly be detected in the images of TbPolIE RNAi depleted cells, even though DAPI staining

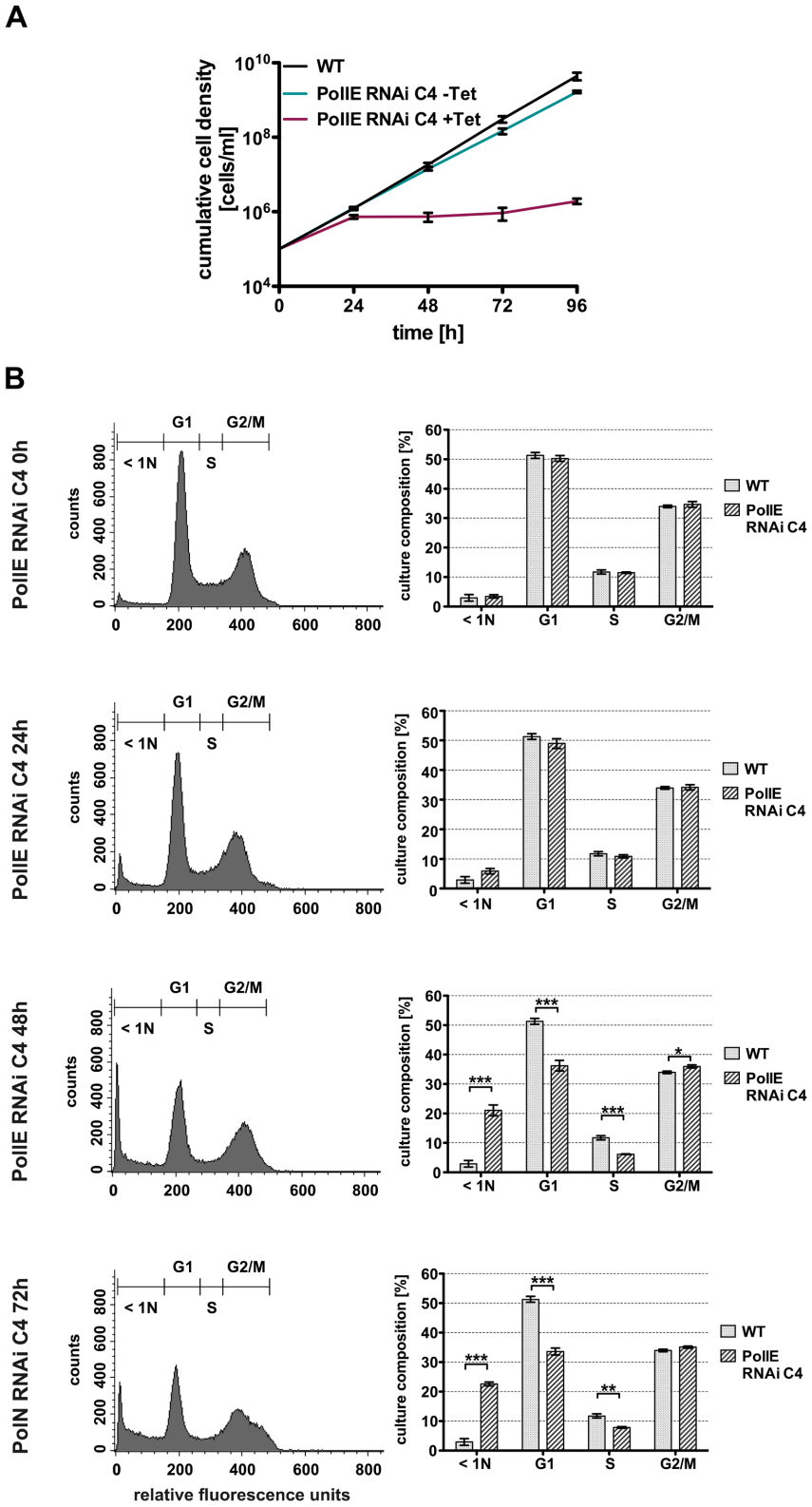

Figure 3. RNAi-depletion of TbPolIE results in growth arrest. (**A**) Cumulative cell density of the parental *T. brucei* RNAi strain 2T1 (WT), TbPolIE RNAi cells grown without addition of tetracycline (Tet–), and TbPolIE RNAi cells after induction of RNAi with tetracycline (Tet+). Error bars denote the standard deviation ($n = 3$). (**B**) Cell cycle profiles of propidium iodide-stained parasites 0, 24, 48 and 72 h after after RNAi-mediated depletion of PolIE (left panel). Graphs display one representative analysis from three experimental repeats. Gates define parasite populations in different cell cycle positions (G1, S and G2/M-phase) or cells with a DNA content less than a diploid cell (<1N). Right panel shows quantification of all three replicates. Parental cell line (WT) served as a control (*$P < 0.05$; **$P < 0.01$; ***$P < 0.0001$, unpaired *t*-test).

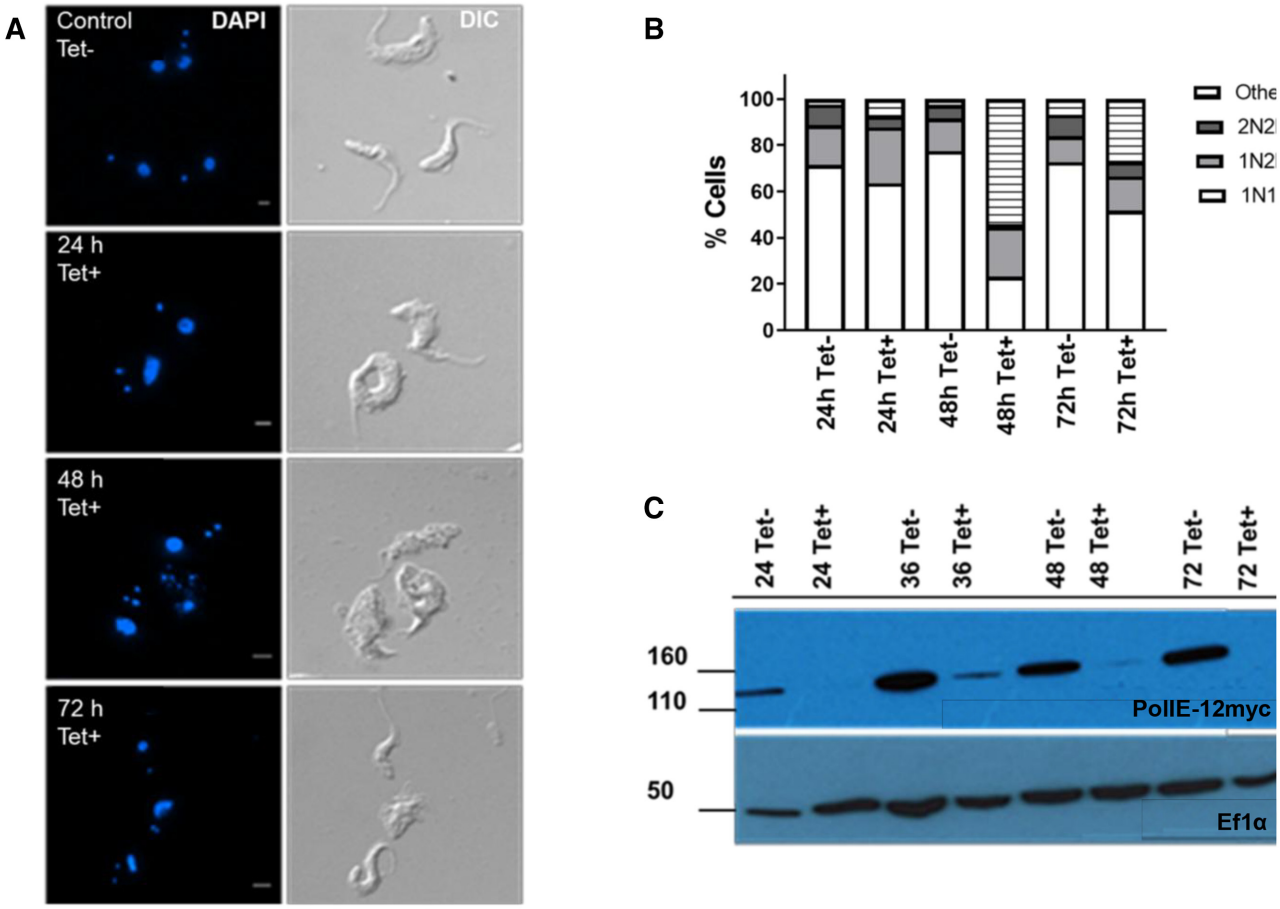

Figure 4. Analysis of the cell cycle after RNAi depletion of TbPolIE. (**A**) Cell cycle analysis by DAPI staining after 24, 48 and 72 h growth in the absence (Tet-) or presence (Tet+) of tetracycline RNAi induction. Immunofluorescence analysis allowing the visualization of the DNA content, and the cell body was visualized by differential interference contrast microscopy (DIC). (**B**) Classification of Tet + and Tet– cells as 1N1K (G1/S), 1N2K (G2/M) and 2N2K (mitosis) cells at the time points shown; 'others' denotes cells that deviate from these classifications. Values depict the mean of each classification in the total population in two biological replicates. More than 200 cells were counted at each time point and in each experiment. (**C**) Western blot analysis using anti-myc antiserum to evaluate abundance of TbPolIE-12myc after 24, 48 and 72 h growth in Tet– and Tet+ cultures; detection of EF1α provides a loading control.

suggested this DNA was present. However, cells with multiple flagellar pockets were seen. Since in *T. brucei* the kinetoplast is connected to the flagellum basal body (73), the number of kinetoplasts is normally directly related with the number of flagellar pockets, perhaps suggesting that DAPI imaging did indeed detect multiple kinetoplasts after depletion of TbPolIE. The SEM images support this observation and reinforce the suggestion of aberrant cell division after TbPolIE loss, since multiple flagella were readily detected in single cells. RNAi induced cells also presented irregular nuclei. Though this phenotype was not detected in all cells, it is consistent with aberrant nuclear staining with DAPI and suggests problems associated with replication or division of the nucleus. Finally, swollen 'vacuole-like' structures were found in a few cells. These structures seemed to be lacking any content and how they arose is unclear.

Loss of TbPolIE results in nuclear damage in some cells

In *T. brucei* and *Leishmania* it has been demonstrated that Thr130 phosphorylation of histone H2A occurs in the presence of diverse types of damage (69) and in gene mutants (15,31,74), indicating this H2A modification is the kinetoplastid variant of serine phosphorylation of either H2A or the H2Ax variant in other eukaryotes. To assess the levels and distribution of γH2A after TbPolIE RNAi, both immunofluorescence and western blotting were performed (Figure 6). Western analysis revealed that expression of γH2A was greater at both 24 and 48 h after TbPolIE RNAi relative to uninduced cells. Immunofluorescence showed that a small amount of nuclear γH2A signal was seen in some uninduced cells, consistent with previous studies. After RNAi, only a modest increase in γH2A signal was seen in some cells after 24 h, whereas a substantially stronger signal was seen 48 h post RNAi induction (Figure 6, Supplementary Figure S6). Nevertheless, even 48 h after RNAi not every cell showed clear γH2A signal, and the level of nuclear anti-γH2A staining varied substantially between cells (Supplementary Figure S6), indicating the levels of nuclear damage resulting from loss of TbPolIE were not uniform across the population. Seventy-two hours after RNAi γH2A signal decreased relative to the 48 h (Figure 6), mirroring the DAPI analysis of cell cycle changes (Figure 4).

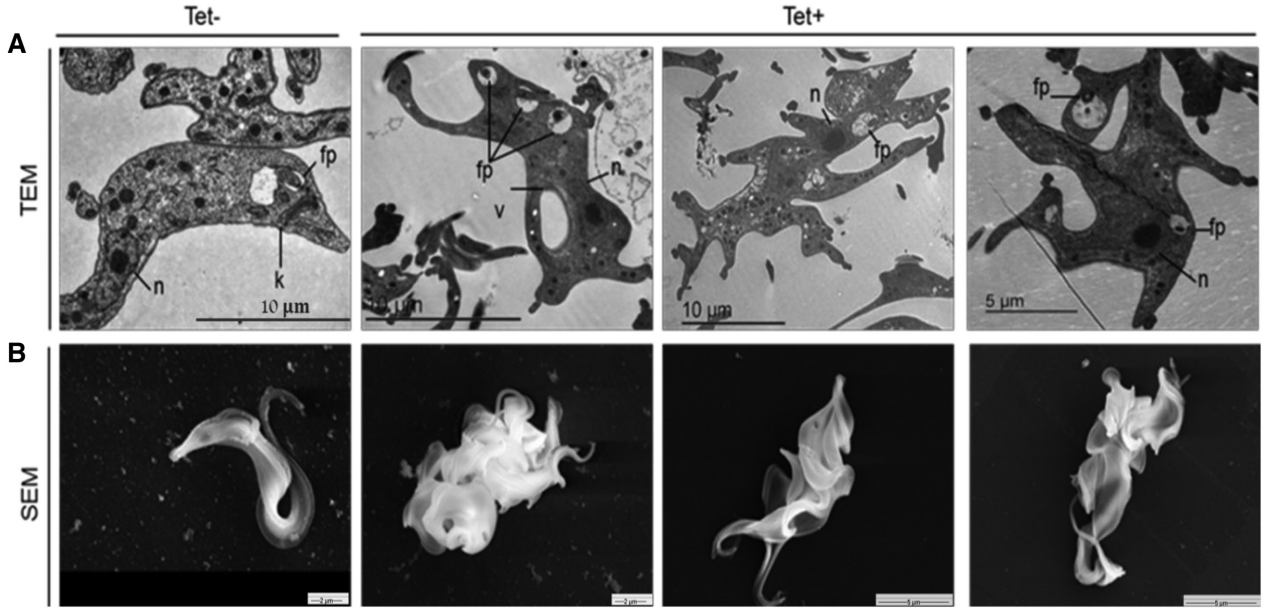

Figure 5. TbPolIE loss is associated with aberrant cell morphology. (**A**) Transmission electron microscopy images of *T. brucei* bloodstream forms before and after RNAi induction. The first panel shows a cell with a regular architecture, before the depletion of TbPolIE (Tet–). Next three panels show representative images of aberrant cells 48 h post RNAi induction (Tet+), presenting abnormal internal architecture. Important features of the cells are indicated in black (n – nucleus; fp – flagellar pocket and v – vacuole). (**B**) Scanning electron microscopy images of *T. brucei* cells. The left panel shows a BSF *T. brucei* cell before RNAi induction (Tet–). The other three panels show representative images of aberrant cells 48 h post RNAi induction of TbPolIE (Tet+).

Depletion of TbPolIE affects nuclear DNA replication

The above data reveal that nuclear damage accumulation, cell cycle abnormalities and a decrease in cell proliferation are all the result of RNAi depletion of TbPolIE. One explanation for this range of phenotypes might be a role of the putative TLS Pol during nuclear genome replication, with genome instability when the protein is lost. To assess a role for TbPolIE during DNA replication the capacity of the cells to incorporate EdU after TbPolIE RNAi was assessed (Figure 7). The cells used in this assay were not synchronized and so were incubated with EdU for 4 h, on the basis that many cells should have undergone at least some DNA synthesis, assuming a nuclear S phase duration of around 1.5 h (75). To allow comparison with EdU uptake after RNAi, the proportion of Tet-induced EdU positive cells at each time point was calculated relative to the uninduced cells at the same time point. A decrease in the number of EdU stained cells (22%) was detected 36 h after RNAi induction, and this became more pronounced after 48 h (when 45% of the population failed to incorporate EdU). These data suggest that DNA replication is impaired after TbPolIE loss and concomitant with the emergence of cell cycle defects and accumulation of DNA damage.

Accumulation of DNA damage after TbPolIE loss cannot simply be explained by impaired DNA replication

To ask if the accumulation of nuclear γH2A and impairment of DNA replication after TbPolIE loss are linked, RNAi cells were grown for 48 h with tetracycline, stained for EdU uptake and simultaneously evaluated for γH2A expression by immunofluorescence (Figure 7C, D). In the uninduced population, where few cells displayed γH2A signal, many had taken up EdU, meaning most (but not all) were negative for the former marker and positive for the latter. In contrast, many cells could be detected after TbPolIE RNAi that did not display EdU signal but had γH2A signal (Figure 7C, D, Supplementary Figure S6); indeed, this was commonly observed in aberrant cells. In addition, some cells without γH2A could be detected that had incorporated EdU (Figure 7C, D, Supplementary Figure S6). Though these patterns may be consistent with stalling of nuclear DNA replication in those TbPolIE RNAi cells that accumulate nuclear damage, cells were also detected, albeit less frequently, which were positive for both EdU and γH2A (Figure 7C, D). These latter cells suggest that a simple cause and effect, such as genome damage resulting from TbPolIE loss leading to impairment of DNA replication and growth, or vice versa, is not clear.

Loss of TbPolIE results in aberrant chromosome segregation in a subset of cells

The severity of the phenotypes observed after RNAi depletion of TbPolIE prompted us to test for loss of chromosome integrity. In order to do so, a telomere-fluorescence *in situ* hybridization (Telo-FISH) assay was performed on TbPolIE RNAi cells after 24 and 48 h with and without RNAi induction (Figure 8). In addition to 11 pairs of large megabase-chromosomes, the genome of *T. brucei* contains approximately 100 small mini-chromosomes. Because mini-chromosomes are more abundant than megabase-chromosomes, it is likely that most of the signal seen using a telomere probe corresponds to the former molecules. As seen in previous work (76), in uninduced RNAi cells, telomere signal was seen diffusely around the nucleus during in-

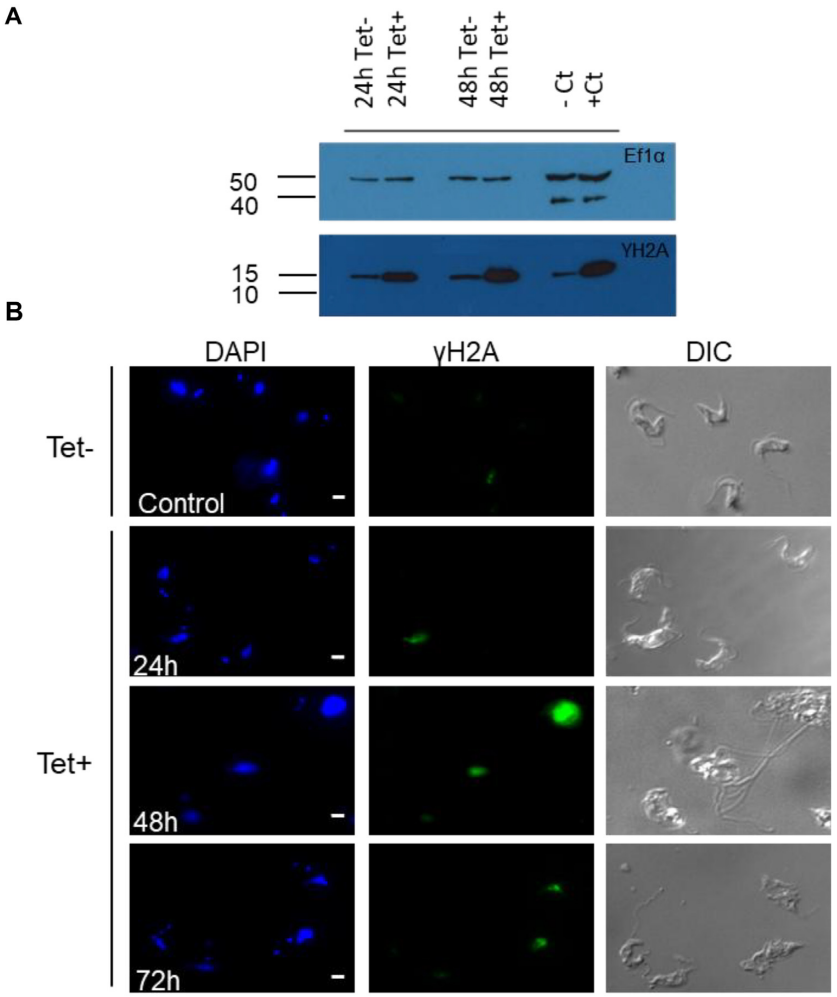

Figure 6. Increase in *T. brucei* γH2A after RNAi of TbPolIE. (**A**) Western blot showing γH2A levels after RNAi depletion of TbPolIE relative to uninduced cells. Signal is shown after 24 and 48 h of growth with (Tet+) or without (Tet–) RNAi induction, and detected with anti-γH2A antiserum. WT cells in the absence and presence of phleomycin (2.5 μg ml^{-1}) were used as negative (–Ct) and positive (+Ct) controls, respectively. Anti-Ef1α antiserum was used as a loading control. Size markers (kDa) are shown. (**B**) Immunolocalization of *T. brucei* γH2A: left panels show DAPI staining of the nucleus and kinetoplast, the middle panels shows γH2A detected with anti-γH2A antiserum, and the right panel show the cell outline by DIC. Representative images are shown of cells 24, 48 and 72 h after RNAi induction, or without induction (Tet–). Scale bar represents 2 μm.

terphase, with a stronger signal towards the nuclear envelope (77). During metaphase the telomeres were found in the centre of the nucleus, and during anaphase the telomeres localized toward the nuclear poles (76,77). From 24 h after RNAi induction, corresponding with the emergence of growth arrest, cell cycle abnormalities and DNA damage, cells with aberrant telomere signals could be seen (Figure 8, further examples Supplementary Figure S7). Most interphase cells appeared comparable with the controls, whereas the typical telomere distribution during metaphase was often absent after RNAi, with cells detected that lacked the expected signal at the equator of the nucleus. During anaphase the ordered segregation of the telomeres into each of the two progeny cells could also be seen to be compromised, with unequal distribution of signal in the nuclei. Finally, telomere distribution was notably unusual in aberrant cells, which were mainly seen after 48 h of RNAi and whose N-K content meant their stage in the cell cycle was unclear. Taken together, these data may be explained by inaccurate chromosome segregation events during mitosis in some cells after loss of TbPolIE, which appears concomitant with the emergence of cells with abnormal N–K ratios and consistent with loss of the putative TLS Pol not impeding mitosis.

Loss of TbPolIE leads to increased expression of silent VSG genes

Given our previous demonstration that TbPolIE binds to chromatin containing telomeric repeats (16), and the above evidence that loss of TbPolIE can affect telomere distribution during nuclear division, we next asked if loss of TbPolIE affects the expression of VSGs from telomeric bloodstream VSG expression sites (Figure 9 and Supplementary Figure S8). Whole cell lysates were prepared at different time points after induction of RNAi and analyzed with antibodies specific for VSG-2, VSG-3 or VSG-13. The parental cell line used to derive the RNAi cells used here encodes only VSG-2 (Figure 10), and the same predominant expression of this VSG was seen at time 0, with levels of VSG-2 only seen to decrease slightly 72 h post induc-

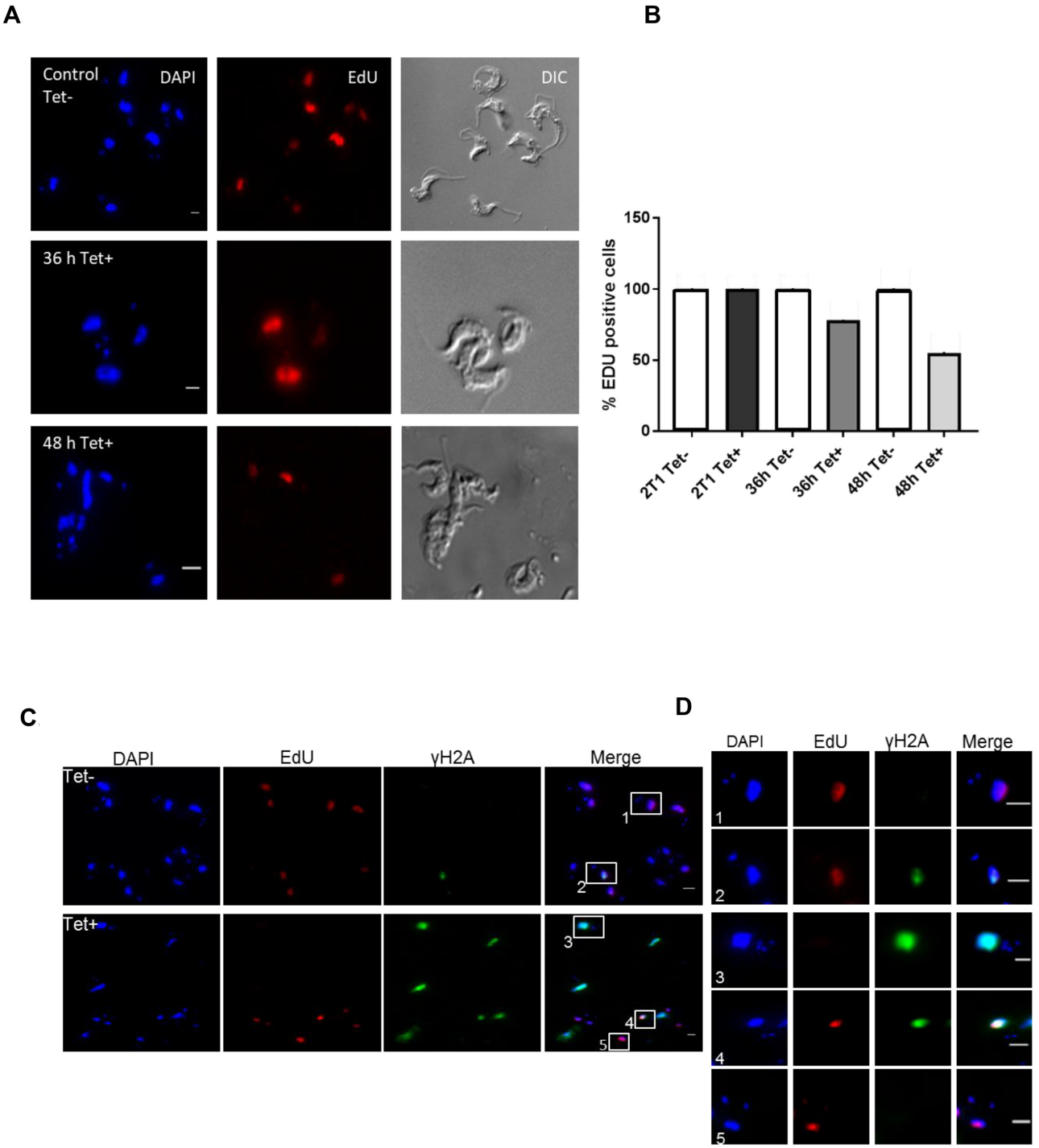

Figure 7. EdU labelling suggests impaired nuclear DNA replication and increased DNA damage after loss of TbPolIE. (**A**) Left panels show DAPI staining of the nucleus and kinetoplast, middle panels show EdU signal, and right panels show the cell outline by DIC. Representative images are shown of cells without RNAi induction (Control, Tet–) and after 36 or 48 h of growth after RNAi induction (Tet+). (**B**) EdU positive cells without (Tet-) or with (Tet+) tetracycline were quantified after 36 and 48 h of growth; the graph depicts the percentage of the total population with EdU signal, comparing the TbPolIE RNAi induced cells at each time point with the same cells grown without Tet (set at 100%); parental 2T1 cells treated in the same way and grown for 48 h are also shown. A minimum of 100 cells were analysed per time point and bars represent mean values of two biological repetitions. (**C**) Cells are shown after 48 h growth in the absence (Tet–) or presence (Tet+) of tetracycline RNAi induction. The first panels (left to right) show DAPI staining of the nucleus and kinetoplast, second panels show γH2A signal detected with anti-γH2A antiserum, third panels show EdU signal, and the fourth panels show a merge of the γH2A and EdU signals. (**D**) Larger images of boxed areas show various patterns of the two nuclear signals seen in uninduced (Tet-) and induced (Tet+) cells: (1) cells showing EdU incorporation and lacking γH2A signal; (2) cells showing overlapping EdU and γH2A signal; (3) cells lacking EdU signal but showing accumulation of damage; (4) cells with overlapping γH2A and EdU signal and (5) cells incorporating EdU and not showing γH2A signal. Scale bar 2 μm.

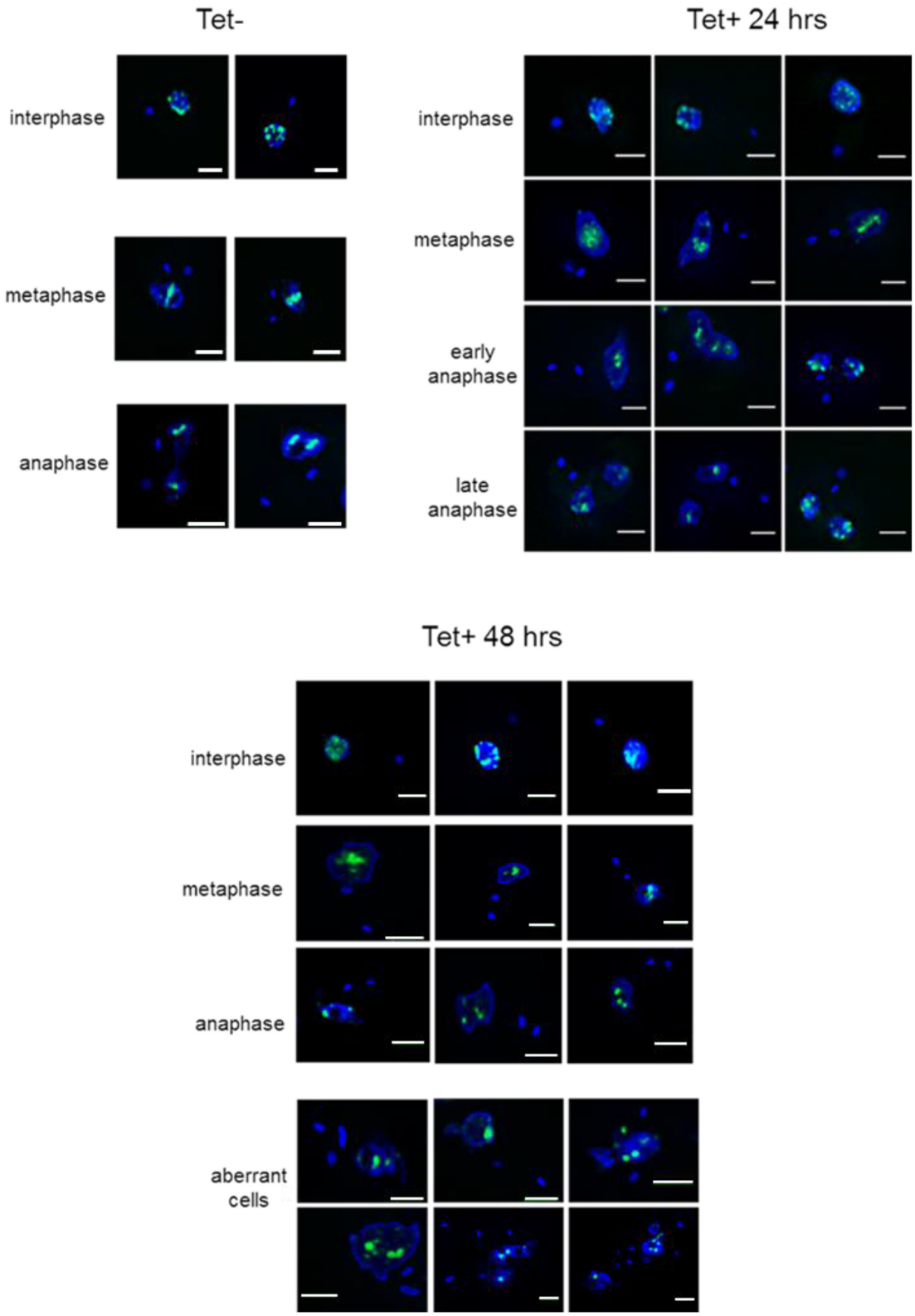

Figure 8. Loss of TbPolIE affects chromosome segregation during cell division. Fluorescence *in situ* hybridization using telomeres as a probe (green) 24 or 48 h after tetracycline induction of RNAi against TbPolIE (Tet+), or in the absence of tetracycline RNAi induction (Tet–). Representative images are shown of cells in interphase, metaphase and anaphase (separated into early or late stages for Tet+ 24 h cells), as well as aberrant cells whose cell cycle phase is unclear. DNA is stained with DAPI; scale bars: 2 μm.

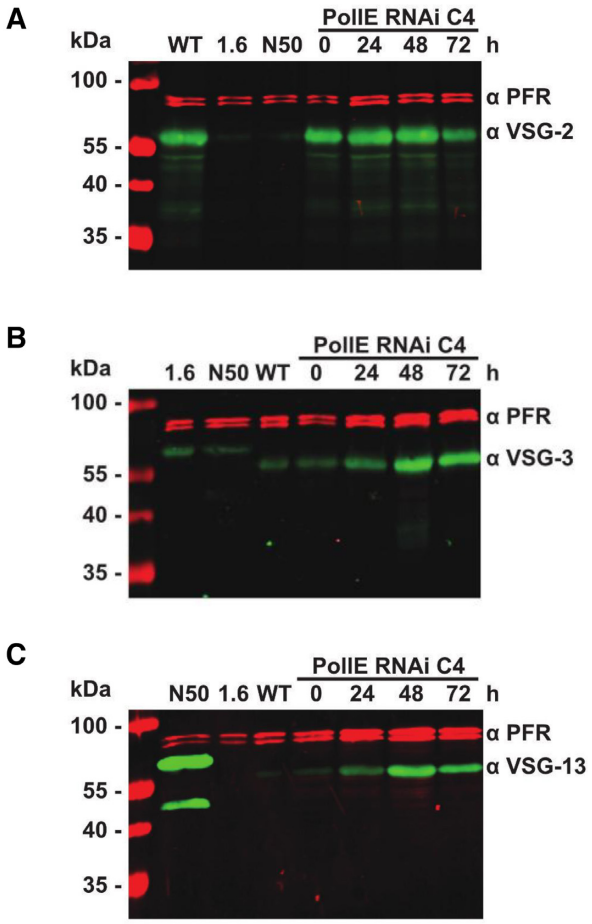

Figure 9. Increased expression of silent VSGs after RNAi depletion of TbPolIE. Whole cell lysates were prepared at different time points after induction of RNAi against TbPolIE in one clone (C4) and probed, after blotting, with antibodies specific for VSG-2 (**A**), VSG-3 (**B**) and VSG-13 (**C**). Antiserum against paraflagellar rod protein (PFR) was used as loading control. In addition, VSG levels were evaluated in a number of control cell lines: MiTat1.2 cells (WT) express VSG-2, whereas M1.6 (MITat1.6) express VSG-6, and N50 express VSG-13.

tion (Figure 9A). In contrast, RNAi induction led to a clear increase in signal for VSG-3 or VSG-13, which are normally transcriptionally repressed in this *T. brucei* strain and were barely detected at time 0. Intriguingly, the extent of the expression of both normally silent VSGs was highest 48 hr post induction, consistent with the dynamics of the cell cycle and DNA damage effects described above. The same effects of increased expression of normally silent VSGs were clearly detectable in another, independent RNAi cell line (Supplementary Figure S8), which suggests either derepression of silent VSG genes or increased switching induced by TbPolIE depletion.

Mass spectrometry analysis shows increased expression of VSGs from throughout the silent archive after TbPolIE depletion

Although the VSG antibodies used in the previous experiment are specific for the VSGs that were used for immunization, it is entirely unclear if and to what extent they can bind to other VSGs. Hence, it is impossible to determine if other deregulated VSGs might contribute to the western blot signals. To attempt to distinguish between loss of transcriptional control and increased switching by recombination, we sought to determine the range of VSGs that become expressed in TbPolIE-depleted parasites with an unbiased approach. To do so, we used a recently published protocol (78) to isolate and characterize the abundance of VSGs from two independent TbPolIE RNAi cell lines 48 and 72 h after RNAi induction by mass spectrometry (Figure 10). Parental 2T1 cells were analysed as a negative control and, like the uninduced RNAi cells, mainly expressed VSG-2 and showed only very minor traces of VSG-8 expression. In contrast, we could detect several VSGs after depletion of TbPolIE. In all samples, the abundance of VSG-8, as well as VSGs from several further BES, including VSG-6, VSG-17 and VSG-11, increased (Figure 10 and Table 2). In addition, substantial increased levels were detected of VSG-653, which is present in a metacyclic VSG expression site (MES) and normally only expressed in the tsetse fly. Finally, we could identify increased abundance of several VSG, such as VSG-636 and VSG-336, which are located in sub-telomeric regions of chromosomes 8 and 9 and not within a BES or MES. Individual data sets of four replicates of two independent clones are presented in Supplementary Figure S9.

Taken together, these data suggest that increased VSG expression after loss of TbPolIE may not simply result from derepression of normally silent telomeric VSG genes in the BES and, perhaps, the MES. The observation that VSGs from the silent, subtelomeric arrays are also found to increase may suggest that loss of TbPolIE also increases recombination events between subtelomeric VSG genes and the BES.

DISCUSSION

Translesion DNA Pols, in addition to allowing cells to grow and survive in the presence of hard to repair genome lesions, are increasingly implicated in wider genome functions, including in various repair pathways (79,80), telomere homoeostasis (81,82) and timing of DNA replication (53). In this work, we have explored the functions of TbPolIE in *T. brucei* and document that this putative TLS Pol, in addition to having important roles in genome maintenance, acts in antigenic variation, a strategy for immune evasion found in a diverse array of bacterial, fungal and protozoan pathogens.

Characterization of TbPolIE in *T. brucei* suggests more work is needed to understand the evolutionary history of this enzyme within the kinetoplastid lineage and its relationship with PolQ and PolIN in other eukaryotes. The fact that the protein is found in the nucleus, and that its loss leads to number of nuclear genome-associated changes, suggests genome maintenance roles related to PolQ and PolIN enzyme functions described in metazoans. However, the PolQ-related protein complement of *T. brucei* (and, it seems, all kinetoplastids) is highly unusual, since the parasite does not encode a 'true' PolQ protein with both DNA Pol and helicase domains, but encodes two related, but discrete DNA Pol and DNA helicase proteins (Figure 1). Thus, *T. brucei* and related kinetoplastids are the only organisms other

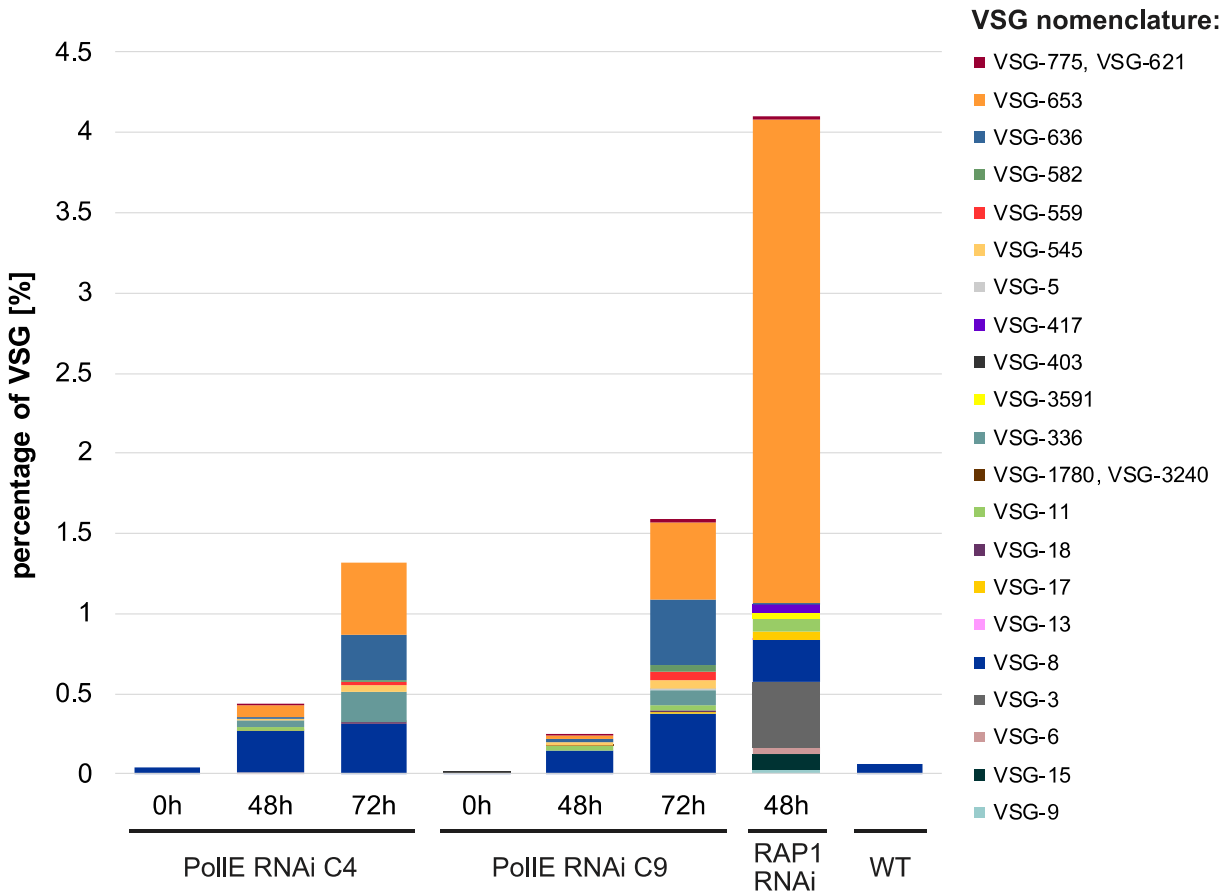

Figure 10. Mass spectrometry reveals increased expression of multiple silent VSGs after TbPolIE loss. The graph shows VSGs identified by mass spectrometry 0, 48 and 72 h after induction of RNAi against TbPolIE. Data is shown for two RNAi clones (C4 and C9), VSG identifiers are coloured, and VSG abundance in the different time points is shown as percentage representation in the samples. VSG-2 is not shown as it displayed an abundance of 95–98% in each sample. The parental 2T1 (WT) cell line was analysed as negative control, and VSGs expressed after 48 h of TbRAP1 RNAi, which is known to result in de-repression of inactive VSG BESs is shown for comparison.

Table 2. Summary of VSG proteins detected by mass spectrometry and their localization in the genome

VSG	Localization in ES	length of ES	Localization in the genome
VSG-6	BES-3	∼47 kb	MBC 4
VSG-8	BES-12	∼42 kb	MBC 2
VSG-17	BES-13	∼52 kb	IC
VSG-18	BES-5	∼42 kb	MBC 5
VSG-11	BES-15	∼58 kb	MBC 3
VSG-1780, VSG-3240			Unknown
VSG-336			3′-STR MBC 8
VSG-403			3′-STR MBC 1
VSG-5			3′-STR MBC 8
VSG-545			3′-STR MBC 8
VSG-559			5′-STR MBC 9
VSG-582	Atypical MES		3′-STR MBC 5
VSG-636			5′-STR MBC 9
VSG-653	MES		5′-STR MBC 11
VSG-775, VSG-621			Unknown, 3′-STR MBC 10

BES: bloodstream form expression sites; MES: metacylic form expression site; MBC: mega base chromosomes; IC intermediate chromosomes; STR: sub-telomeric region.

than metazoans to possess genes encoding separate DNA Pol (64) and helicase proteins related to PolQ (83), and the only organisms so far detailed that express only these proteins and not PolQ.

PolQ is present in more eukaryotic species than PolN, perhaps suggesting the former protein is ancestral (59) and that only some eukaryotes have undergone gene fission to generate a stand-alone PolN. This may explain the PolQ-related, but structurally PolN-like genes seen in *Dictyostelium discoideum* and *Thalassiosira pseudonana*, though in neither case has function been explored. Indeed, the absence of neither PolQ nor PolN in several eukaryotes may suggest the functions provided by these Pols have been discarded several times during evolution. In all cases, how retention or discarding of PolQ and PolN relates to the presence or absence of a separate HelQ protein deserves further consideration, particularly since HelQ-like, but not PolQ- or PolN-like, proteins have been described in archaea (62,63), and *C. elegans* and *D. melanogaster* encode PolQ and HelQ-like proteins but not PolN. In this context, the distinct grouping of TbPolIE as one apparent paralogue of five kinetoplastid genes encoding only a Pol domain, and the presence of an isolated HelQ-like protein in all kinetoplastids, muddies any clarity in understanding the evo-

lution of these seemingly connected proteins. For instance, did TbPolIA-E arise as an expansion of bacterial PolI in kinetoplastids in order to manage the complex mitochondrial genome, with TbPolIE then diverging to provide nuclear functions? Alternatively, are these enzymes descendants of eukaryotic PolQ due to gene fission, with most paralogues diverted to the mitochondrion? Again, any link between TbPolIE and the putative kinetoplastid HelQ protein deserves further analysis, since *Trypanosoma* and *Leishmania* parasites display robust microhomology-mediated end-joining activity (84–86), an activity that has so far been ascribed only to PolQ in other eukaryotes (49–52). Currently, the only work on the putative kinetoplastid HelQ has been in *T. cruzi*, where the factor has been implicated in DNA replication, not repair (83). Thus, we do not know if kinetoplastid PolIE and the putative HelQ function together, as has been suggested for PolN and HelQ (Hel308) in human cells (58). Relatively little work has explored the functions of PolN in other eukaryotes, but null mutants of the gene are viable in mice (59) and loss of PolN has been described to affect meiotic recombination, with conflicting evidence for the protein having a role in tackling cross-link DNA damage (58,59). Thus, the seemingly more severe effects of loss of TbPolIE we describe in *T. brucei* compared with PolN mutation mice and human cells may reflect retention of some PolQ-like roles in the parasite.

The *L. infantum* orthologue of TbPolIE has been shown to display TLS activity (64) and, assuming the *T. brucei* protein retains this activity, our analysis of TbPolIE represents just the second functional examination of a TLS Pol in *T. brucei*. Perhaps surprisingly, both TLS Pols are critical for growth of the parasite in culture. Previously, Rudd *et al*. examined two Prim-Pol proteins in *T. brucei*, called TbPPL1 and TbPPL2 (15). Loss of TbPPL2 by RNAi, like loss of TbPolIE, dramatically impairs cell growth and leads to accumulation of damage. However, several lines of evidence suggest that the proteins perform distinct functions. First, TbPolIE-12myc displays a striking localization mainly in two peripheral regions of the nucleus, whereas no such discrete accumulation of TbPPL2 was described. Second, though loss of both Pols results in increased γH2A signal in the nucleus, indicating accumulation of damage, the modified histone is seen as multiple foci after TbPPL2 RNAi, whereas after TbPolIE loss γH2A signal is not clearly focal and displays considerable variation between cells. Third, though loss of TbPolIE caused redistribution of the Pol in the nucleoplasm after alkylation damage by MMS, we found limited evidence for recruitment of the protein to the resulting γH2A foci, unlike the pronounced overlap of γH2A and TbPPL2 seen after MMS exposure. Finally, whereas loss of TbPPL2 resulted in a striking stall of cell division at G2/M, loss of TbPolIE appears instead to have a less severe impediment to cell cycle progression, since cells with aberrant DNA content arise after RNAi that are indicative of inaccurate genome segregation after mitosis. It is conceivable that this difference in cell cycle response explains why loss of TbPPL2 appears to have a more severe effect on cell growth than loss of TbPolIE. However, it is less clear why the cell cycle and DNA damage defects that arise after loss of TbPolIE peak 48 h after RNAi and then diminish; whether this indicates adaptation of the cells, such as by increased use of an alternative TLS Pol, or if the effectiveness of RNAi is more rapidly lost after depletion of TbPolIE, is unclear. Despite such disparate activities, the fact that loss of either protein results in such pronounced loss of cell viability is striking, since it indicates endogenous genome features in *T. brucei* that must be tackled by TLS Pols for effective genome transmission during cell division. What such endogenous genome features might be is unknown. TbPPL2 has been shown to allow replication bypass of base cross-links generated by UV and 8-oxoG formed by oxidation, but is not capable of bypassing 3dMeA or an abasic site (15). LiPolQ (LiPolIE) shares some but not all of these catalytic activities: like TbPPL2 it can bypass 8-oxoG, but is also capable of crossing an abasic site (64). Whether any of these activities underlie the important, endogenous roles played by the TLS Pols is unknown, and we cannot exclude the possibility that the defects seen after loss of either protein reflect a shared and hitherto undescribed role. Notably, previous analysis did not ask if loss of TbPPL2 affects VSG expression, as we describe after RNAi of TbPolIE.

Our previous work revealed association of TbPolIE with the *T. brucei* telomere (16), but what role it may play was not tested. To date, neither PolQ nor PolN have not been associated with telomere homeostasis in any eukaryote, though TLS Pol eta activity has been shown to contribute to alternative lengthening of telomeres in mammalian cells (81), where it may contribute to recombination (87). Analysis of the potential roles of kinetoplastid TLS Pols in recombination is so far limited to *T. cruzi* (88,89), without examining the telomere. Our data show that loss of TbPolIE results in changes in expression of VSG genes that are found adjacent to the telomere with evidence for increased expression of VSGs in BES and MES, as well as from subtelomeric array VSGs. We cannot say if these alterations are due to an impact of TbPolIE loss on telomere maintenance, but the effects on VSG expression controls have some similarity with those seen after loss of *T. brucei* shelterin components, including TbRAP1, TbTRF and TbTIF2. All three of these telomeric factors are essential for trypanosome viability. However, while TbTRF and TbTIF2 only play minor roles in VSG silencing, TbRAP1 is critical for BES-linked VSG suppression (23). Depletion of TbRAP1 leads to derepression of all silent BESs, with the most prominent effect at telomere-proximal regions. In addition, a recent study (32) revealed that TbRAP1 loss leads to increased readthrough into the telomere downstream of the active BES, resulting in higher levels of non-coding telomeric repeat-containing RNAs (TERRA) and telomeric RNA:DNA hybrids. In addition, more DSBs were detected at telomeres and subtelomeres of active and silent BESs, which increased the VSG switching frequency by initiating VSG gene conversion. In contrast, depletion of TbTRF and TbTIF2 did not affect TbRAP1-mediated VSG silencing, but resulted in increased gene conversion-mediated VSG switching events (26), which appeared to rely on independent and overlapping mechanisms, since TbTIF2 knockdown leads to the accumulation of subtelomeric DSBs, an effect not seen after TbTRF depletion. This mechanistic overlap may arise because TbTIF2 stabilizes TbTRF protein levels by suppressing its degradation by the 26S proteasome (26). In summary, although TbTRF, TbTIF2 and TbRAP1 are components

of the same complex, only TbRAP1 is crucial for telomeric VSG silencing, suggesting that TbTIF2 and TbTRF act independently from TbRAP1, which is supported by yeast two-hybrid studies that reveal only a weak interaction between TbRAP1 and TbTRF (23), but a very strong interaction of TbTRF and TbTIF2 (25).

Given the above complexity in VSG switching functions of the three known telomere-associated factors in *T. brucei*, it is possible that TbPolIE also contributes to telomere stability and its ablation leads to damage that undermines monoallelic VSG expression and/or leads to VSG recombination. Such a telomere-directed function would be consistent with our previous demonstration that TbPolIE binds chromatin-associated telomeric repeats (16), and the observation here that RNAi against TbPolIE alters telomere localization. However, other explanations might also be considered. One alternative possibility is that TbPolIE plays a direct role in VSG switching, such as during replication of the VSG BES or contributing to VSG recombination. For instance, TbPolIE may play an important role in overcoming impediments to replication that are found in the VSG BES and, in its absence, damage accumulates and increases VSG switching. What such impediments might be are unclear, but RNA-DNA hybrids (31) and a modified base (J) (90) have been described in the VSG BES, as well as elsewhere in the genome (31,91). If TbPolIE were to play a catalytic role in VSG recombination, perhaps through a PolQ-like function in microhomology-mediated end-joining, it is unclear why its depletion would lead to the observed increases in silent VSG expression, rather than impeding changes in VSG expression. A wider explanation may be that loss of TbPolIE affects genome replication, which then deregulates the controls that normally ensure monoallelic VSG expression. For instance, it is known that the active VSG BES, unlike all the silent BESs, is replicated early in S phase (27). If S phase progression or the correct segregation of chromosomes were perturbed, it is conceivable that such targeted replication of only the active BES might breakdown, leading to changes in VSG transcription or recombination in all VSG BES. Such a replication-focused explanation may explain why similar effects on VSG expression are seen after depletion of the factors involved in DNA replication, including the Origin Recognition Complex (28,29) and MCM-BP (30). However, whether such effects are due to global problems with genome replication, or are due to VSG BES-focused roles is difficult to separate. However, in this regard, two observations are worth noting. First, RNAi depletion of TbPPL2 does not lead to detectable effects on VSG expression (data not shown), which may be because loss of this TLS Pol prevents transition from G2/M into mitosis (15), unlike the cell cycle perturbations seen after loss of TbPolIE. Second, recent data have implicated HelQ of *T. cruzi* in DNA replication (83); if such a role is conserved in *T. brucei*, and if trypanosomatid HelQ and PolIE proteins work together, then a link between VSG switching and genome replication might be more firmly established.

DATA AVAILABILITY

The mass spectrometry proteomics data have been deposited to the ProteomeXchange Consortium via the PRIDE [1] partner repository with the dataset identifier PXD015648.

SUPPLEMENTARY DATA

Supplementary Data are available at NAR Online.

ACKNOWLEDGEMENTS

Author contributions: R.M., F.B. and C.J.J. designed the study. A.Z.L., M.S., E.B., H.R., N.W., J.W. and L.L. performed the bioinformatics analysis, bio-imaging and cell biology analysis of the TbPolIE-depleted parasites. K.L. and F.B. performed the mass spectrometry analysis. R.M., F.B. and C.J.J. wrote the manuscript. All authors read and approved the final manuscript.

FUNDING

Work in the Butter and Janzen laboratories was supported by a joint DFG research grant [BU2996/13-1, JA1013/6-1]; Work in the McCulloch laboratory was supported by the BBSRC [BB/K006495/1, BB/M028909/1, BB/N016165/1, DTP studentship to E.B.]; SENESCYT (Secretaria Nacional de Educación Superior, Ciencia y Tecnología e Innovación) PhD scholarship (to A.L.); The Wellcome Centre for Integrative Parasitology is supported by core funding from the Wellcome Trust [104111]. Funding for open access charge: DFG [JA 1013/6-1].
Conflict of interest statement. None declared.

REFERENCES

1. Cotterill,S. and Kearsey,S. (2009) Eukaryotic DNA polymerases. In: *Encyclopedia of Life Sciences (ELS)*. John Wiley & Sons, Ltd., Chichester, pp. 1–6.
2. Raia,P., Delarue,M. and Sauguet,L. (2019) An updated structural classification of replicative DNA polymerases. *Biochem. Soc. Trans.*, **47**, 239–249.
3. Powers,K.T. and Washington,M.T. (2018) Eukaryotic translesion synthesis: choosing the right tool for the job. *DNA Repair (Amst.)*, **71**, 127–134.
4. Vaisman,A. and Woodgate,R. (2017) Translesion DNA polymerases in eukaryotes: what makes them tick? *Crit. Rev. Biochem. Mol. Biol.*, **52**, 274–303.
5. Goodman,M.F. and Woodgate,R. (2013) Translesion DNA polymerases. *Cold Spring Harb. Perspect. Biol.*, **5**, a010363.
6. Kunkel,T.A. (2004) DNA replication fidelity. *J. Biol. Chem.*, **279**, 16895–16898.
7. Sale,J.E. (2013) Translesion DNA synthesis and mutagenesis in eukaryotes. *Cold Spring Harb. Perspect. Biol.*, **5**, a012708.
8. Iyama,T. and Wilson,D.M. 3rd (2013) DNA repair mechanisms in dividing and non-dividing cells. *DNA Repair (Amst.)*, **12**, 620–636.
9. Gao,Y., Mutter-Rottmayer,E., Zlatanou,A., Vaziri,C. and Yang,Y. (2017) Mechanisms of post-replication DNA repair. *Genes (Basel)*, **8**, 64.
10. Andersen,P.L., Xu,F. and Xiao,W. (2008) Eukaryotic DNA damage tolerance and translesion synthesis through covalent modifications of PCNA. *Cell Res.*, **18**, 162–173.
11. Zhuang,Z. and Ai,Y. (2010) Processivity factor of DNA polymerase and its expanding role in normal and translesion DNA synthesis. *Biochim. Biophys. Acta*, **1804**, 1081–1093.
12. Boehm,E.M., Spies,M. and Washington,M.T. (2016) PCNA tool belts and polymerase bridges form during translesion synthesis. *Nucleic Acids Res.*, **44**, 8250–8260.
13. Wojtaszek,J., Lee,C.J., D'Souza,S., Minesinger,B., Kim,H., D'Andrea,A.D., Walker,G.C. and Zhou,P. (2012) Structural basis of

Rev1-mediated assembly of a quaternary vertebrate translesion polymerase complex consisting of Rev1, heterodimeric polymerase (Pol) zeta, and Pol kappa. *J. Biol. Chem.*, **287**, 33836–33846.
14. Mailand,N., Gibbs-Seymour,I. and Bekker-Jensen,S. (2013) Regulation of PCNA-protein interactions for genome stability. *Nat. Rev. Mol. Cell Biol.*, **14**, 269–282.
15. Rudd,S.G., Glover,L., Jozwiakowski,S.K., Horn,D. and Doherty,A.J. (2013) PPL2 translesion polymerase is essential for the completion of chromosomal DNA replication in the African trypanosome. *Mol. Cell*, **52**, 554–565.
16. Reis,H., Schwebs,M., Dietz,S., Janzen,C.J. and Butter,F. (2018) TelAP1 links telomere complexes with developmental expression site silencing in African trypanosomes. *Nucleic Acids Res.*, **46**, 2820–2833.
17. Duraisingh,M.T. and Horn,D. (2016) Epigenetic regulation of virulence gene expression in parasitic protozoa. *Cell Host Microbe*, **19**, 629–640.
18. Cross,G.A.M. (1975) Identification, purification and properties of clone-specific glycoprotein antigens constituting the surface coat of *Trypanosoma brucei*. *Parasitology*, **71**, 393–417.
19. Berriman,M., Ghedin,E., Hertz-Fowler,C., Blandin,G., Renauld,H., Bartholomeu,D.C., Lennard,N.J., Caler,E., Hamlin,N.E., Haas,B. *et al.* (2005) The genome of the African trypanosome Trypanosoma brucei. *Science*, **309**, 416–422.
20. Cross,G.A., Kim,H.S. and Wickstead,B. (2014) Capturing the variant surface glycoprotein repertoire (the VSGnome) of Trypanosoma brucei Lister 427. *Mol. Biochem. Parasitol.*, **195**, 59–73.
21. Hertz-Fowler,C., Figueiredo,L.M., Quail,M.A., Becker,M., Jackson,A., Bason,N., Brooks,K., Churcher,C., Fahkro,S., Goodhead,I. *et al.* (2008) Telomeric expression sites are highly conserved in Trypanosoma brucei. *PLoS One*, **3**, e3527.
22. McCulloch,R., Morrison,L.J. and Hall,J.P.J. (2015) DNA recombination strategies during antigenic variation in the African Trypanosome. *Microbiol. Spectr.*, **3**, MDNA3-0016-2014.
23. Yang,X., Figueiredo,L.M., Espinal,A., Okubo,E. and Li,B. (2009) RAP1 is essential for silencing telomeric variant surface glycoprotein genes in Trypanosoma brucei. *Cell*, **137**, 99–109.
24. Jehi,S.E., Li,X., Sandhu,R., Ye,F., Benmerzouga,I., Zhang,M., Zhao,Y. and Li,B. (2014) Suppression of subtelomeric VSG switching by Trypanosoma brucei TRF requires its TTAGGG repeat-binding activity. *Nucleic Acids Res.*, **42**, 12899–12911.
25. Jehi,S.E., Wu,F. and Li,B. (2014) Trypanosoma brucei TIF2 suppresses VSG switching by maintaining subtelomere integrity. *Cell Res.*, **24**, 870–885.
26. Jehi,S.E., Nanavaty,V. and Li,B. (2016) Trypanosoma brucei TIF2 and TRF suppress VSG switching using overlapping and independent mechanisms. *PLoS One*, **11**, e0156746.
27. Devlin,R., Marques,C.A., Paape,D., Prorocic,M., Zurita-Leal,A.C., Campbell,S.J., Lapsley,C., Dickens,N. and McCulloch,R. (2016) Mapping replication dynamics in Trypanosoma brucei reveals a link with telomere transcription and antigenic variation. *Elife*, **5**, e12765.
28. Tiengwe,C., Marcello,L., Farr,H., Dickens,N., Kelly,S., Swiderski,M., Vaughan,D., Gull,K., Barry,J.D., Bell,S.D. *et al.* (2012) Genome-wide analysis reveals extensive functional interaction between DNA replication initiation and transcription in the genome of Trypanosoma brucei. *Cell Rep.*, **2**, 185–197.
29. Benmerzouga,I., Concepcion-Acevedo,J., Kim,H.S., Vandoros,A.V., Cross,G.A., Klingbeil,M.M. and Li,B. (2013) Trypanosoma brucei Orc1 is essential for nuclear DNA replication and affects both VSG silencing and VSG switching. *Mol. Microbiol.*, **87**, 196–210.
30. Kim,H.S. (2019) Genome-wide function of MCM-BP in Trypanosoma brucei DNA replication and transcription. *Nucleic Acids Res.*, **47**, 634–647.
31. Briggs,E., Crouch,K., Lemgruber,L., Lapsley,C. and McCulloch,R. (2018) Ribonuclease H1-targeted R-loops in surface antigen gene expression sites can direct trypanosome immune evasion. *PLoS Genet.*, **14**, e1007729.
32. Nanavaty,V., Sandhu,R., Jehi,S.E., Pandya,U.M. and Li,B. (2017) Trypanosoma brucei RAP1 maintains telomere and subtelomere integrity by suppressing TERRA and telomeric RNA:DNA hybrids. *Nucleic Acids Res.*, **45**, 5785–5796.
33. Glover,L., Alsford,S. and Horn,D. (2013) DNA break site at fragile subtelomeres determines probability and mechanism of antigenic variation in African trypanosomes. *PLoS Pathog.*, **9**, e1003260.
34. Huson,D.H. and Bryant,D. (2006) Application of phylogenetic networks in evolutionary studies. *Mol. Biol. Evol.*, **23**, 254–267.
35. Hamming,R.W. (1950) Error detecting and error correcting codes. *Bell Syst. Tech.J.*, **24**, 147–160.
36. Bryant,D. and Moulton,V. (2004) Neighbor-net: an agglomerative method for the construction of phylogenetic networks. *Mol. Biol. Evol.*, **21**, 255–265.
37. Saitou,N. and Nei,M. (1987) The neighbor-joining method: a new method for reconstructing phylogenetic trees. *Mol. Biol. Evol.*, **4**, 406–425.
38. Gower,J.C. (1966) Some distance properties of latent root and vector methods used in multivariate analysis. *Biometrika*, **53**, 325.
39. Holland,B. and Moulton,V. (2003) Consensus networks: a method for visualising incompatibilities in collections of trees. *Algorith. Bioinformatics Proc.*, **2812**, 165–176.
40. Dress,A.W. and Huson,D.H. (2004) Constructing splits graphs. *IEEE/ACM Trans. Comput. Biol. Bioinform.*, **1**, 109–115.
41. Figueiredo,L.M., Janzen,C.J. and Cross,G.A. (2008) A histone methyltransferase modulates antigenic variation in African trypanosomes. *PLoS Biol.*, **6**, e161.
42. Stortz,J.A., Serafim,T.D., Alsford,S., Wilkes,J., Fernandez-Cortes,F., Hamilton,G., Briggs,E., Lemgruber,L., Horn,D. and Mottram,J.C. (2017) Genome-wide and protein kinase-focused RNAi screens reveal conserved and novel damage response pathways in Trypanosoma brucei. *PLoS Pathog.*, **13**, e1006477.
43. Alsford,S. and Horn,D. (2008) Single-locus targeting constructs for reliable regulated RNAi and transgene expression in Trypanosoma brucei. *Mol. Biochem. Parasitol.*, **161**, 76–79.
44. Jones,N.G., Thomas,E.B., Brown,E., Dickens,N.J., Hammarton,T.C. and Mottram,J.C. (2014) Regulators of Trypanosoma brucei cell cycle progression and differentiation identified using a Kinome-Wide RNAi screen. *PLoS Pathog.*, **10**, e1003886.
45. Yousefzadeh,M.J. and Wood,R.D. (2013) DNA polymerase POLQ and cellular defense against DNA damage. *DNA Repair (Amst.)*, **12**, 1–9.
46. Seki,M., Masutani,C., Yang,L.W., Schuffert,A., Iwai,S., Bahar,I. and Wood,R.D. (2004) High-efficiency bypass of DNA damage by human DNA polymerase Q. *EMBO J.*, **23**, 4484–4494.
47. Hogg,M., Seki,M., Wood,R.D., Doublie,S. and Wallace,S.S. (2011) Lesion bypass activity of DNA polymerase theta (POLQ) is an intrinsic property of the pol domain and depends on unique sequence inserts. *J. Mol. Biol.*, **405**, 642–652.
48. Yoon,J.H., Roy Choudhury,J., Park,J., Prakash,S. and Prakash,L. (2014) A role for DNA polymerase theta in promoting replication through oxidative DNA lesion, thymine glycol, in human cells. *J. Biol. Chem.*, **289**, 13177–13185.
49. Chan,S.H., Yu,A.M. and McVey,M. (2010) Dual roles for DNA polymerase theta in alternative end-joining repair of double-strand breaks in Drosophila. *PLos Genet.*, **6**, e1001005.
50. Mateos-Gomez,P.A., Gong,F., Nair,N., Miller,K.M., Lazzerini-Denchi,E. and Sfeir,A. (2015) Mammalian polymerase theta promotes alternative NHEJ and suppresses recombination. *Nature*, **518**, 254–257.
51. Koole,W., van Schendel,R., Karambelas,A.E., van Heteren,J.T., Okihara,K.L. and Tijsterman,M. (2014) A polymerase theta-dependent repair pathway suppresses extensive genomic instability at endogenous G4 DNA sites. *Nat. Commun.*, **5**, 3216.
52. Roerink,S.F., van Schendel,R. and Tijsterman,M. (2014) Polymerase theta-mediated end joining of replication-associated DNA breaks in C. elegans. *Genome Res.*, **24**, 954–962.
53. Fernandez-Vidal,A., Guitton-Sert,L., Cadoret,J.C., Drac,M., Schwob,E., Baldacci,G., Cazaux,C. and Hoffmann,J.-S. (2014) A role for DNA polymerase theta in the timing of DNA replication. *Nat. Commun.*, **5**, 4285.
54. Takata,K., Shimizu,T., Iwai,S. and Wood,R.D. (2006) Human DNA polymerase N (POLN) is a low fidelity enzyme capable of error-free bypass of 5S-thymine glycol. *J. Biol. Chem.*, **281**, 23445–23455.
55. Yamanaka,K., Minko,I.G., Takata,K., Kolbanovskiy,A., Kozekov,I.D., Wood,R.D., Rizzo,C.J. and Lloyd,R.S. (2010) Novel enzymatic function of DNA polymerase nu in translesion DNA synthesis past major groove DNA-peptide and DNA-DNA cross-links. *Chem. Res. Toxicol.*, **23**, 689–695.
56. Takata,K., Arana,M.E., Seki,M., Kunkel,T.A. and Wood,R.D. (2010) Evolutionary conservation of residues in vertebrate DNA

polymerase N conferring low fidelity and bypass activity. *Nucleic Acids Res.*, **38**, 3233–3244.
57. Zietlow,L., Smith,L.A., Bessho,M. and Bessho,T. (2009) Evidence for the involvement of human DNA polymerase N in the repair of DNA interstrand cross-links. *Biochemistry*, **48**, 11817–11824.
58. Moldovan,G.L., Madhavan,M.V., Mirchandani,K.D., McCaffrey,R.M., Vinciguerra,P. and D'Andrea,A.D. (2010) DNA polymerase POLN participates in cross-link repair and homologous recombination. *Mol. Cell. Biol.*, **30**, 1088–1096.
59. Takata,K.I., Reh,S., Yousefzadeh,M.J., Zelazowski,M.J., Bhetawal,S., Trono,D., Lowery,M.G., Sandoval,M., Takata,Y., Lu,Y. *et al.* (2017) Analysis of DNA polymerase nu function in meiotic recombination, immunoglobulin class-switching, and DNA damage tolerance. *PLos Genet.*, **13**, e1006818.
60. Muzzini,D.M., Plevani,P., Boulton,S.J., Cassata,G. and Marini,F. (2008) Caenorhabditis elegans POLQ-1 and HEL-308 function in two distinct DNA interstrand cross-link repair pathways. *DNA Repair (Amst.)*, **7**, 941–950.
61. Richards,J.D., Johnson,K.A., Liu,H., McRobbie,A.M., McMahon,S., Oke,M., Carter,L., Naismith,J.H. and White,M.F. (2008) Structure of the DNA repair helicase hel308 reveals DNA binding and autoinhibitory domains. *J. Biol. Chem.*, **283**, 5118–5126.
62. Guy,C.P. and Bolt,E.L. (2005) Archaeal Hel308 helicase targets replication forks in vivo and in vitro and unwinds lagging strands. *Nucleic Acids Res.*, **33**, 3678–3690.
63. Northall,S.J., Buckley,R., Jones,N., Penedo,J.C., Soultanas,P. and Bolt,E.L. (2017) DNA binding and unwinding by Hel308 helicase requires dual functions of a winged helix domain. *DNA Repair (Amst.)*, **57**, 125–132.
64. Fernandez-Orgiler,A., Martinez-Jimenez,M.I., Alonso,A., Alcolea,P.J., Requena,J.M., Thomas,M.C., Blanco,L. and Larraga,V. (2016) A putative Leishmania DNA polymerase theta protects the parasite against oxidative damage. *Nucleic Acids Res.*, **44**, 4855–4870.
65. Milton,M.E., Choe,J.Y., Honzatko,R.B. and Nelson,S.W. (2016) Crystal structure of the apicoplast DNA polymerase from plasmodium falciparum: the first look at a plastidic A-Family DNA polymerase. *J. Mol. Biol.*, **428**, 3920–3934.
66. Klingbeil,M.M., Motyka,S.A. and Englund,P.T. (2002) Multiple mitochondrial DNA polymerases in Trypanosoma brucei. *Mol. Cell*, **10**, 175–186.
67. Miller,J.C., Delzell,S.B., Concepcion-Acevedo,J., Boucher,M.J. and Klingbeil,M.M. (2020) A DNA polymerization-independent role for mitochondrial DNA polymerase I-like protein C in African trypanosomes. *J. Cell Sci.*, **133**.
68. Goos,C., Dejung,M., Janzen,C.J., Butter,F. and Kramer,S. (2017) The nuclear proteome of Trypanosoma brucei. *PLoS One*, **12**, e0181884.
69. Glover,L. and Horn,D. (2012) Trypanosomal histone gammaH2A and the DNA damage response. *Mol. Biochem. Parasitol.*, **183**, 78–83.
70. Siegel,T.N., Hekstra,D.R. and Cross,G.A. (2008) Analysis of the Trypanosoma brucei cell cycle by quantitative DAPI imaging. *Mol. Biochem. Parasitol.*, **160**, 171–174.
71. Hammarton,T.C. (2007) Cell cycle regulation in Trypanosoma brucei. *Mol. Biochem. Parasitol.*, **153**, 1–8.
72. Monnerat,S., Clucas,C., Brown,E., Mottram,J.C. and Hammarton,T.C. (2009) Searching for novel cell cycle regulators in Trypanosoma brucei with an RNA interference screen. *BMC Res Notes*, **2**, 46.
73. Sunter,J.D. and Gull,K. (2016) The flagellum attachment zone: 'the cellular ruler' of Trypanosome morphology. *Trends Parasitol.*, **32**, 309–324.
74. Damasceno,J.D., Obonaga,R., Silva,G.L.A., Reis-Cunha,J.L., Duncan,S.M., Bartholomeu,D.C., Mottram,J.C., McCulloch,R. and Tosi,L.R.O. (2018) Conditional genome engineering reveals canonical and divergent roles for the Hus1 component of the 9-1-1 complex in the maintenance of the plastic genome of Leishmania. *Nucleic Acids Res.*, **46**, 11835–11846.
75. Woodward,R. and Gull,K. (1990) Timing of nuclear and kinetoplast DNA replication and early morphological events in the cell cycle of *Trypanosoma brucei*. *J. Cell Sci.*, **95**, 49–57.
76. DuBois,K.N., Alsford,S., Holden,J.M., Buisson,J., Swiderski,M., Bart,J.-M., Ratushny,A.V., Wan,Y., Bastin,P., Barry,J.D. *et al.* (2012) NUP-1 Is a large coiled-coil nucleoskeletal protein in trypanosomes with lamin-like functions. *PLoS Biol.*, **10**, e1001287.
77. Ogbadoyi,E., Ersfeld,K., Robinson,D., Sherwin,T. and Gull,K. (2000) Architecture of the *Trypanosoma brucei* nucleus during interphase and mitosis. *Chromosoma*, **108**, 501–513.
78. Glover,L., Hutchinson,S., Alsford,S. and Horn,D. (2016) VEX1 controls the allelic exclusion required for antigenic variation in trypanosomes. *Proc. Natl Acad. Sci. U.S.A.*, **113**, 7225–7230.
79. Henrikus,S.S., van Oijen,A.M. and Robinson,A. (2018) Specialised DNA polymerases in Escherichia coli: roles within multiple pathways. *Curr. Genet.*, **64**, 1189–1196.
80. McVey,M., Khodaverdian,V.Y., Meyer,D., Cerqueira,P.G. and Heyer,W.D. (2016) Eukaryotic DNA polymerases in homologous recombination. *Annu. Rev. Genet.*, **50**, 393–421.
81. Garcia-Exposito,L., Bournique,E., Bergoglio,V., Bose,A., Barroso-Gonzalez,J., Zhang,S., Roncaioli,J.L., Lee,M., Wallace,C.T., Watkins,S.C. *et al.* (2016) Proteomic profiling reveals a specific role for translesion DNA polymerase eta in the alternative lengthening of telomeres. *Cell Rep.*, **17**, 1858–1871.
82. Tsai,H.H., Shu,H.W., Yang,C.C. and Chen,C.W. (2012) Translesion-synthesis DNA polymerases participate in replication of the telomeres in Streptomyces. *Nucleic Acids Res.*, **40**, 1118–1130.
83. de Lima,L.P., Calderano,S.G., da Silva,M.S., de Araujo,C.B., Vasconcelos,E.J.R., Iwai,L.K., Pereira,C.A., Fragoso,S.P. and Elias,M.C. (2019) Ortholog of the polymerase theta helicase domain modulates DNA replication in Trypanosoma cruzi. *Sci. Rep.*, **9**, 2888.
84. Conway,C., Proudfoot,C., Burton,P., Barry,J.D. and McCulloch,R. (2002) Two pathways of homologous recombination in *Trypanosoma brucei*. *Mol. Microbiol.*, **45**, 1687–1700.
85. Burton,P., McBride,D.J., Wilkes,J.M., Barry,J.D. and McCulloch,R. (2007) Ku heterodimer-independent end joining in Trypanosoma brucei cell extracts relies upon sequence microhomology. *Eukaryot. Cell*, **6**, 1773–1781.
86. Glover,L., McCulloch,R. and Horn,D. (2008) Sequence homology and microhomology dominate chromosomal double-strand break repair in African trypanosomes. *Nucleic Acids Res.*, **36**, 2608–2618.
87. McIlwraith,M.J., Vaisman,A., Liu,Y., Fanning,E., Woodgate,R. and West,S.C. (2005) Human DNA polymerase eta promotes DNA synthesis from strand invasion intermediates of homologous recombination. *Mol. Cell*, **20**, 783–792.
88. de Moura,M.B., Schamber-Reis,B.L., Passos Silva,D.G., Rajao,M.A., Macedo,A.M., Franco,G.R., Pena,S.D.J., Teixeira,S.M.R. and Machado,C.R. (2009) Cloning and characterization of DNA polymerase eta from Trypanosoma cruzi: roles for translesion bypass of oxidative damage. *Environ. Mol. Mutagen.*, **50**, 375–386.
89. Rajao,M.A., Passos-Silva,D.G., DaRocha,W.D., Franco,G.R., Macedo,A.M., Pena,S.D.J., Teixeira,S.M. and Machado,C.R. (2009) DNA polymerase kappa from Trypanosoma cruzi localizes to the mitochondria, bypasses 8-oxoguanine lesions and performs DNA synthesis in a recombination intermediate. *Mol. Microbiol.*, **71**, 185–197.
90. van Leeuwen,F., Wijsman,E.R., Kieft,R., van der Marel,G.A., van Boom,J.H. and Borst,P. (1997) Localization of the modified base J in telomeric VSG gene expression sites of *Trypanosoma brucei*. *Genes Dev.*, **11**, 3232–3241.
91. Borst,P. and Sabatini,R. (2008) Base J: discovery, biosynthesis, and possible functions. *Annu. Rev. Microbiol.*, **62**, 235–251.